Reply to Reviewer #1

We thank the Reviewer for carefully reviewing our manuscript and providing insightful comments. Below we address each comment point by point. For clarity we mark the reviewer comment in **blue**, our answers in **black**, and changes to the manuscript in **red**. Page and line numbers in our replies refer to the revised manuscript.

Secondary organic aerosol (SOA) is an important fraction of aerosol particles in the atmosphere all over the world. However, its formation via different chemical and/or physical processes remains largely unquantified, mostly due to incapacity of separating these pathways. In addition to the traditional measurement of SOA by aerosol mass spectrometry, in which the molecular fingerprint of SOA is seldomly preserved, the recent development of FIGAERO inlet does allow to explore the molecular information. A primary challenge for FIGAERO data analysis is that there are also several processes going on in parallel that is difficult to deconvolute. As also pointed out by the authors, vapor condensation and aerosol-phase (or aqueous-phase chemistry) are occurring simultaneously; the latter alone also contains many different pathways, such as oligomerization, hydrolysis, formation of organic salts, and etc. To address this major challenge in FIGAERO data analysis, the authors applied PMF analysis on such data sets for the first time, which convincibly shows that PMF is able to separate, to a big extent, different parallel processes. Thus, in general, I found this work containing enough new insights and recommend its acceptance in ACP. However, besides these insights, I have several comments to be addressed, as list below:

1. P2 L23-24, ". . .,thus reducing the mass transport limitation which hinders evaporation." This sentence reads ambiguous. It can mean that reducing the mass transport limitation hinders evaporation, which I believe the opposite of what the authors meant. Please rephrase.

The sentence has been rephrased as:

On the one hand, it will act as a plasticiser, reducing the particle viscosity (Renbaum-Wolff et al., 2013; Virtanen et al., 2010) and thus reducing the mass transport limitation in the particles. These transport limitations are responsible for the reduced evaporation under dry conditions.

2. P6 L24-26, Eq. 4-6. The Ratioexp seems to represent the explained fraction of the measured data by PMF. How does this differ from the traditional way of calculating the explained fraction (sum|Rij – Xij|)/(sum|Xij|)? What is the advantage of using this one?

The ratio of explained variance (variation) is a standard parameter used in the analysis of results when expressing measurement data with models. We decided to use this metric in addition to the examination of residuals between the reconstructed and measured data.

The explained, unexplained, and total variance (or variation) are normally calculated with the quadratic distance from the "expected" value (i.e., the average value for each ion i).

35

$$Var_{total} = \sum_{ij} (X_{ij} - \bar{X}_\iota)^2$$

$$Var_{explained} = \sum_{ij} (R_{ij} - \bar{X}_\iota)^2$$

$$Var_{unexplained} = \sum_{ij} (X_{ij} - R_{ij})^2$$

$$Var_{total} = Var_{explained} + Var_{unexplained}$$

Then the ratio between $Var_{explained}$ and Var_{total} can be interpreted as R^2.

40 When using these equations with our data, the sum of $Var_{explained}$ and $Var_{unexplained}$ was not equal to Var_{total}, but much smaller for PMF solutions with low factor number and larger for solutions with higher factor numbers. The latter leads to ratios >1 which are not meaningful in this context. Also, if the calculation was performed in the other dimension, i.e. calculating the variance with respect to the average value for each observation j, the values for $Var_{explained}$ / Var_{total} changed. When using the absolute distances instead of the quadratic this behaviour changed and $Var_{explained} + Var_{unexplained} \approx Var_{total}$. Thus,

45 we decided to use this metric as a compromise.

3. P8 L18, Eq.8. Based on the observation of model residue, you decide to use CNerror instead of PLerror for uncertainty matrix. As shown in Figure S1, CNerror is about 1-2 orders of magnitude smaller than PLerror. However, with the CNerror, Q/Qexp got very close to 1, as shown in Figure S2, which seems to indicate that CNerror is the true error or close to that. Do

50 you have any idea about the reason?

It may be that the overestimation of the error with the PLerror scheme has a stronger impact on the overall Q/Q_{exp} value than the underestimation in the CNerror case.

We observed that adding the blank measurements to the dataset decreased the Q/Q_{exp} values in the CN case. Note that in the low- and medium O:C case (where we had 4 blank measurements) approx. half of the datapoints are dominated by noise as no

55 significant signal was detected.

4. P11, L1-4. It seems that the criterion of justify the type V factors is its little change in Tmax with aerosol age or water content. As the authors stated "But this method can be applied to e.g. ambient FIGAERO-CIMS measurements as well" In the abstract (P2 L5), it is important to suggest how to determine the type V factors when applying PMF on ambient data sets,

60 where aerosol oxidation degree (O:C), aerosol age and water content are often correlated.

The main criterion for V-type factors is indeed the shape and small change in T_{max} in comparison to the B- and D-type factors. This characteristic persists when looking at ambient data. We have just started applying this new method to an ambient dataset which will be the topic of a future publication.

Volatility (or vapour pressure) is primarily controlled by the detailed molecular structure (i.e. functionality) of a compound. There are many different compounds that have similar vapour pressures so they would fall into the same VBS bin or here V-type factor. Assume different compounds A, B, C, D which all have the same order of magnitude C*. If one SOA type contains A and B but no C and D while the other SOA type contains only C and D, a PMF analysis of the thermal desorption data of these two aerosol types will yield two factors with the same T_{max}. One will contain A and B while the other has C and D. What we find a bit surprising is that changing the oxidation field for a single precursor has such a strong effect on the composition. One possible explanation is that the HO_2/RO_2 chemistry may be strongly affected by increasing the OH exposure by an order of magnitude.

Also prompted by the request of Reviewer #3 we decided to add two section in the SI material (1.3 and 1.4) elaborating on the effect of different SOA types on our PMF analysis.

6. P13 L20-23. Likewise, same molecules (e.g., C8H10O5) can be separated into different V factors. Together with Point 5, do these observations suggest that the degree of thermos-decomposition may play an important (even a major) role in the final detected FIGAERO spectra?

For our dataset there are two main reasons why a single detected composition (e.g. C8H10O5) is split over several factor: 1) there is a direct desorption and thermal decomposition part (possibly from a range of different low volatility precursors). 2) there are several conceivable isomers of that composition. Please remember that any 1D mass spectrometer can only provide information on the sum formula of a molecule but not the functionality within the molecule (i.e., the connections between the atoms). This is why we avoid speaking of molecule or compounds in the manuscript.

As we state in the conclusions, thermal decomposition plays an important role for desorption temperatures above ~120 C. This should definitively be considered when analysing integrated FIGAERO-CIMS mass spectra and e.g. using the detected sum formulas in parameterisation to calculate vapour pressure. This has been pointed out also in earlier FIGAERO publications (e.g. Lopez-Hilfiker et al., 2014; Stark et al., 2017). With PMF we can now separate the contribution of direct desorption and thermal decomposition for each detected ion/sum formula.

7. P14 L3-4. Do you have any hint to explain why highOC SOA seems to be more influenced by aqueous-phase chemistry?

We elaborated on possible chemical reactions in our previous publication (Buchholz et al., 2019). Briefly, there we speculate that in the highOC case a larger fraction of organic (hydroxy-)peroxides is present. Those are sensitive to hydrolysis which will initiate a range of reactions in the aqueous phase. As peroxides are also thermally unstable, they are most likely detected as their non-peroxy analogues in FIGAERO-CIMS which complicates interpretations. We now mention this at the start of section 3.3:

As discussed by Buchholz et al. (2019), the different behaviour of the highOC SOA is most likely due to higher fractions of (hydro-)peroxides in the particles caused by the much higher HO_2 concentrations in the OFR at the highOC oxidation conditions. Most peroxides are sensitive to hydrolysis which will initiate a range of reactions in the aqueous phase. The low volatility products of these reactions thermally decompose to similar fragments as did the peroxide precursor. Thus, the same groups of ions are detected but at a higher T_{desorp}.

References

Buchholz, A., Lambe, A. T., Ylisirniö, A., Li, Z., Tikkanen, O. P., Faiola, C., Kari, E., Hao, L., Luoma, O., Huang, W., Mohr, C., Worsnop, D. R., Nizkorodov, S. A., Yli-Juuti, T., Schobesberger, S. and Virtanen, A.: Insights into the O: C-dependent mechanisms controlling the evaporation of α-pinene secondary organic aerosol particles, Atmos. Chem. Phys., 19(6), 4061–4073, doi:10.5194/acp-19-4061-2019, 2019.

Lopez-Hilfiker, F. D., Mohr, C., Ehn, M., Rubach, F., Kleist, E., Wildt, J., Mentel, T. F., Lutz, A., Hallquist, M., Worsnop, D. and Thornton, J. A.: A novel method for online analysis of gas and particle composition: description and evaluation of a Filter Inlet for Gases and AEROsols (FIGAERO), Atmos. Meas. Tech., 7, 983–1001, doi:10.5194/amt-7-983-2014, 2014.

Renbaum-Wolff, L., Grayson, J. W., Bateman, A. P., Kuwata, M., Sellier, M., Murray, B. J., Shilling, J. E., Martin, S. T. and Bertram, A. K.: Viscosity of α-pinene secondary organic material and implications for particle growth and reactivity., Proc. Natl. Acad. Sci. U. S. A., 110(20), 8014–8019, doi:10.1073/pnas.1219548110, 2013.

Stark, H., Yatavelli, R. L. N., Thompson, S. L., Kang, H., Krechmer, J. E., Kimmel, J. R., Palm, B. B., Hu, W., Hayes, P. L., Day, D. A., Campuzano-Jost, P., Canagaratna, M. R., Jayne, J. T., Worsnop, D. R. and Jimenez, J. L.: Impact of Thermal Decomposition on Thermal Desorption Instruments: Advantage of Thermogram Analysis for Quantifying Volatility Distributions of Organic Species, Environ. Sci. Technol., 51(15), 8491–8500, doi:10.1021/acs.est.7b00160, 2017.

Virtanen, A., Joutsensaari, J., Koop, T., Kannosto, J., Yli-Pirilä, P., Leskinen, J., Mäkelä, J. M., Holopainen, J. K., Pöschl, U., Kulmala, M., Worsnop, D. R. and Laaksonen, A.: An amorphous solid state of biogenic secondary organic aerosol particles, Nature, 467(7317), 824–827, doi:10.1038/nature09455, 2010.

Reply to Reviewer #2

We thank the Reviewer for carefully reviewing our manuscript and providing insightful comments. Below we address each comment point by point. For clarity we mark the reviewer comment in **blue**, our answers in **black**, and changes to the manuscript in **red**. Page and line numbers in our replies refer to the revised manuscript.

Summary:

The authors performed positive matrix factorisation on FIGAERO-CIMS data of SOA before and after isothermal evaporation, under both low and high humidity. They provide a detailed description of their methods including two ways of estimating PMF errors, which is useful and interesting. However, I found some of their interpretations to be a bit unconvincing or not completely evaluated. A lot of the analysis revolves around the highOC case under wet conditions, but I have several questions as to the quality of their PMF solutions for that case, and whether the aerosol in that case is even representative of anything that would be present in the atmosphere. The authors also haven't convinced me that PMF of thermograms could provide more information than one could get from single ion thermograms, so more discussion is needed to show how they're actually advancing the field. I think this work could be suitable for publication in ACP if these major revisions can be addressed. I include several major comments as general comments, followed by some more specific and technical comments.

General Comments:

1: Looking at Fig S7, what jumped out at me was that typically all of the factors are decreasing in absolute magnitude after 4 h compared to 0.25 h of evaporation. My first thought was that I would have expected the lower volatility factors to remain more constant, and just the higher volatility factors would evaporate. However, I think you could explain that all factors should lose at least some absolute mass because the total amount of OA will be decreasing, and that will change the equilibrium partitioning causing even the lower volatility compounds to evaporate. I think it could be really interesting if you would calculate how much of each factor you expect to evaporate, using their estimated volatility from the FIGAERO combined with the change in OA mass measured after evaporation, and compare this with how much you measured to evaporate. Do they match? This might be outside the scope of your manuscript, but it wouldn't take too much effort and would add value to the paper if you decide try it. It would give the reader more information with which to judge how well PMF actually is able to separate compounds of different volatilities.

This investigation would be indeed interesting and a good way to verify our interpretation. But this is not possible with the experimental setup that was used for this data set. First, the difference between the total mass collected for t_{evap}=0.25h and 4h does not depend only on the aerosol mass lost in the RTC. The t_{evap}=0.25h sample was collected directly after the size selection unit (and not from the RTC at 0.25h). The total amount collected on the FIGAERO filter depended on the collection time and

the particle concentration in the sample flow. This concentration was 4 – 10 times higher than reached in the RTC after filling. For the t_{evap}=4h samples, the collected mass depended on the aerosol mass filled into the RTC (which was different for the different aerosol types) and how much was lost due to evaporation, wall losses and sampling from the RTC before collection. Second note that there is no equilibrium partitioning inside the RTC as the stainless-steel walls, in practice, act as perfect sinks for the evaporating compounds. This ensures that there is no build-up of organic vapours in the gas phase that would limit the particle evaporation. These experiments were designed to provide optimal input data for process modelling. For future investigations we will consider designing experiments to obtain the data needed to directly investigate the particle mass losses as the reviewer suggests.

2: Following up on my previous comment, one piece of information you've given the reader with which to judge the ability of PMF to separate compounds of different volatilities is table 2, the T_max values for each factor for each experiment. In addition, you've described in the abstract page 1 line 29 how "Thus, the factors identified with PMF could be interpreted as volatility classes." However, I would expect that if PMF is truly separating compounds of similar volatilities into each factor, that the factor would maintain roughly constant T_max (and roughly constant desorption shape) for each of the dry and wet experiments at both evaporation times. I would say that your factors for the lowOC and mediumOC cases maintain roughly the same T_max and shape across all wet/dry and 0.25,4 h cases. The only thing that changes is the magnitudes of the factors. This appears to be supporting evidence of the argument that PMF is separating compounds successfully by volatility. But for the highOC case, it doesn't appear to be successfully separating the volatility factors. The T_max for most of the factors changes substantially between dry and wet cases and after evaporation. This suggests to me that the factors are somewhat blended together. Another thing that leads me to that conclusion is that a lot of the mass gets shifted to the background HB1 factor during the wet,4h case, whereas the HB1 factor was much lower during other highOC cases. A background factor shouldn't change like that from case to case. I don't doubt that it is likely to be aqueous chemistry causing these changes in the PMF factors, but you haven't convinced me that PMF is giving you real and useful information about the process, particularly for the highOC/wet case which you're using as evidence of aqueous chemical changes. Maybe you need to revisit your PMF methods and see if you can find a 'better' solution, otherwise please explain your interpretation of the chosen factors in context of the points I've raised here.

The fact that the T_{max} values are changing together with the appearance of a "new" factor (HWET) is the strongest argument that there are additional processes at work apart from simple isothermal evaporation. Each V-type factor consists of a large number of compounds with similar (but not identical) volatility. In the low- and mediumOC cases, the volatility of the compounds in each V-type factor are similar enough that most of them are affected in a similar fashion by the isothermal evaporation. I.e., a similar fraction of all constituents of a volatile V-type factor evaporate, thus not changing the overall shape and T_{max} value of the factor. (If the grouping of a factor would be too wide (i.e., covering a too broad C* range), isothermal evaporation would result in a change in shape and T_{max} as the more volatile compounds in a factor would have evaporate more than the less volatile ones.) In the highOC case, not all compounds in the volatile factors participate in aqueous phase chemical

2

processes. This will contribute to changes in the shape of the factor profiles of v-type factors and possibly their T_{max} values. It seems that slightly more volatile compounds in each V-type factor (those at slightly lower T_{desorp}) are affected more by the aqueous phase.

70   Regarding the apparent strong increase of HB1 in the wet, t_{evap} = 4h we need to correct the perception of the reviewer. The change in y-axis scaling in Figure 7 is mainly causing this. We have added a note about the different y-axis scaling to the figure description of Figures 5-7 in the main manuscript and S 4 - S 6 and SI material to prevent this misconcenption to happen to future readers.

In Figure R2_1 below, we show the temperature profiles of HB1 for all highOC samples and the blank measurement. The
75   absolute values for all samples are within the same range. This suggests that the "source" for this factor is the instrument itself as the amounts of particular mass collected on the filter in these 5 cases were very different. There is a decrease of the profile between ~50 and 120 °C which is not there for the wet, t_{evap} = 4h and the blank sample. This can be interpreted as part of the background not being separated from the main signal (or factors "blended together"). This is most likely caused by the main factors being so much stronger than the background in that part of the data. Similar behaviour (a dip in the B factor) was also
80   observed some of the in the low- and mediumOC case, but there the effect was not as pronounced has in the highOC case. This can be interpreted as short coming of the PMF method. Some adjusting of the error matrix may help with this. With the used CNerror scheme a relatively higher importance was assigned to strong signals in their peaks.
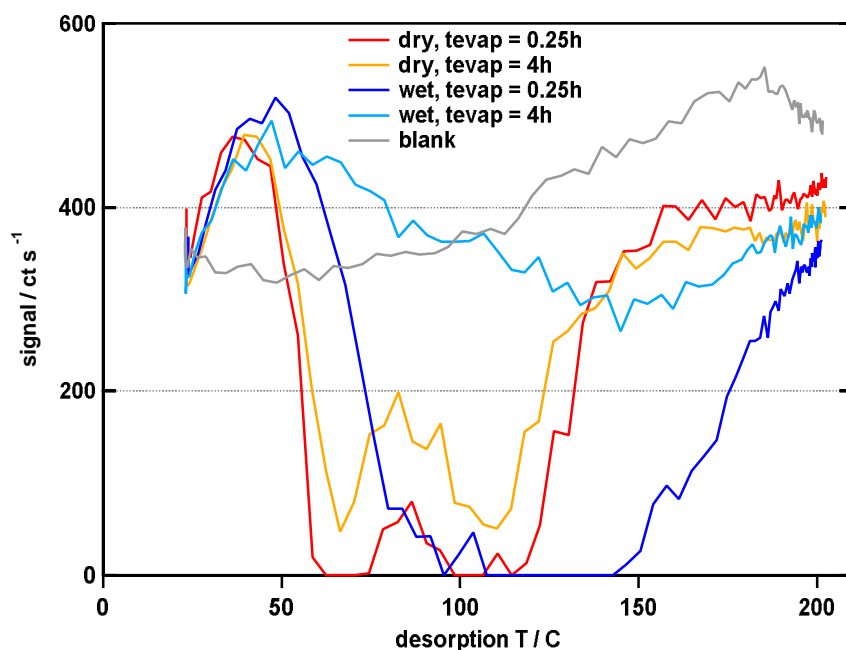

Figure R2_1: Factor profile of HB1 for all highOC samples.

85

3: You have demonstrated that PMF can be useful for pulling out background/contamination signals from thermograms, and also that higher volatility factors evaporate preferentially over lower volatility factors (though you could also say the same using just T_max of total signal). But, I'm not sure I see much discussion of which scientific insights you're gaining by doing PMF on thermograms. E.g., PMF on aerosol mass spectrometer (AMS) data can be used for general source apportionment. All of your aerosol comes from the same source in this particular experiment, but is there any information gained through PMF that could indicate anything about the aerosol formation/evaporation process? Are there factors that can be used as tracers for aqueous chemistry, that could be searched for in ambient datasets? Please expand on how you are making specific scientific advances using thermogram PMF that we can't get using other non-PMF methods.

Thermal decomposition in FIGAERO is one of the major problems of the method when the aim is to identify the detailed composition or volatility of the compounds. One major output of the PMF analysis which is not accessible from simple analysis of the thermograms is the contribution of thermal decomposition to the overall signal. Without PMF, we can only speculate that a broader peak, a shoulder, or a tail is caused by thermal decomposition of larger compounds. Especially broadening may also be cause by instrument artefacts. Schobesberger et al. (2018) use a modelling approach to capture the contribution of "reversible oligomers" (i.e. thermally decomposing compounds) on an ion by ion basis. But there estimates for several physical parameters (e.g. enthalpy of evaporation) are needed for each ion. PMF does not need any such assumptions to identify that fraction of a single ion thermogram that stems most likely from thermal decomposition. Knowing about the thermal decomposition is extremely important when using data from FIGAERO-CIMS (or any other instrument involving treatment at elevated temperatures) with sum formula based parametrisation (e.g. DeRieux et al., 2018; Li et al., 2016) or for modelling applications. The companion paper (Tikkanen et al., 2019) shows an example of how the output of this type of PMF analysis can be combined with detailed process modelling.

We cannot provide a simple tracer for aqueous phase chemistry in the atmosphere as this dataset was limited to a-pinene SOA formed under specific conditions. But the PMF analysis directly revealed the presence of aqueous phase chemistry in the highOC case and identified the ions affected by the process. In the original analysis of the data (Buchholz et al., 2019), we had to combine multiple features in the dataset that just "did not add up" (e.g. very little change in apparent volatility from isothermal evaporation but a strong change in the thermograms) and then manually inspect hundreds of single ion thermograms to realise that besides the simple isothermal evaporation there was a different process dominating the composition changes in the high OC case.

The next step with this method is clearly the application to ambient datasets. First, preliminary results are suggesting that the PMF analysis does separate different ambient sources for the SOA and provides valuable insights into the volatility of those sources.

We expanded the discussion in the conclusion part including more information on how the presented method improves the interpretation of FIGAERO-CIMS measurements and thus increases our understanding of the aerosol composition.

To maintain the context of these additions, we provide here the full paragraph from the Conclusion section highlighting the additions in **bold.**

120 PMF was able to separate the measured signal of each ion into instrument background, contamination, and collected aerosol mass. This separation worked even if no filter blank data was added to the datasets. However, adding filter blank measurements to the dataset simplified the identification of background factors. Identifying background factors in this way instead of simply subtracting periodically taken filter blank measurements is especially helpful, if an insufficient number of filter blank measurements were collected or if the background changed between filter blank samples. **Being able to determine the actual**

125 **contribution of background compounds becomes even more important for low concentration measurements (i.e., low collected sample mass on the FIGAERO filter). The shape of the combined thermogram of the background may significantly alter the overall shape of the thermogram (e.g., shift the T_{max} value) and thus change the interpretation of the volatility of the collected aerosol.**

The collected aerosol mass signal part was separated into (mostly) direct desorption factors (i.e., volatility classes) and thermal

130 decomposition factors. Thermal decomposition became the dominant process for many low M_w ions observed at temperatures above 120 °C. Then the observed "desorption" temperatures are actually the decomposition temperatures and thus give an upper limit for the true volatility of the parent compounds. This shows again that FIGAERO-CIMS measurements may overestimate the volatility of aerosol particles based on parameterisation of the overall composition but also on desorption temperatures as described by some previous studies (Lopez-Hilfiker et al., 2016; Schobesberger et al., 2018; Stark et al., 2017).

135 **The knowledge about the contribution of thermal decomposition to a thermogram measurement obtained with the PMF method presented here can be used e.g. to improve the input into process models. An example for such an application is presented in Tikkanen et al. (2019).**

For each SOA type (i.e., α-pinene SOA of different oxidative age) 5 main volatility classes were identified in the chosen PMF solution. Isothermal evaporation prior to sampling with FIGAERO-CIMS systematically removed the more volatile factors

140 with T_{max} values corresponding to SVOCs. Low M_w compounds remaining in the particles after evaporation were attributed to low volatility factors indicating that they most likely were products of thermal decomposition above ~100 °C. However, between ~100 and 120 °C thermal decomposition was still a minor process. In the highOC case, the aqueous phase chemistry occurring under wet conditions was captured by introducing a new factor and shifts in T_{max} for other factors. Both the educts and products (or thermal decomposition products of them) could be identified. This highlights how PMF analysis can help

145 with identifying processes in the particle phase.

The highOC SOA in our study may not be representative of ambient SOA of the same OC ratio as it was formed under extremely strong oxidation conditions in an OFR. But the type of compounds affected by aqueous phase chemistry (i.e., organic compounds containing (hydro)peroxides or other functional groups which easily hydrolyse and then continue to react) are not unique to OFR reactors. One formation path of compounds containing several hydroperoxyl or

150 **peroxiacid groups is the auto-oxidation of terpenes in the gas-phase leading to highly oxygenated material (HOM) (Bianchi et al., 2019; Ehn et al., 2014). These compounds play an important role in particle growth and detected more and more in ambient measurements (Lee et al., 2018; Mohr et al., 2017). Another compound class which is possibly susceptible to hydrolysis is organo-nitrates (which did not occur in our study due to the experiment design). Thus,**

ambient aerosol will probably not show as clear signs of aqueous phase chemistry as our high OC case, but it is very
likely that such processes occur to some degree and may be detected with the PMF analysis of FIGAERO thermogram
data.

…

The example ions shown in Figure 9 highlight how important it is to allow a single ion to contribute to more than one class/factor when analysing FIGAERO-CIMS data. Clustering techniques, as for example described by Koss et al. (2019) or Li et al. (2019), which assign each detected ion/composition to a single cluster, are incapable of capturing such a behaviour, i.e., the shift of T_{max} between two measured thermograms due to the selective removal of some of the isomers/thermal decomposition products. For the investigated dataset, we artificially removed the volatile fraction at a set ion composition with the prior isothermal evaporation. However, as the composition of ambient aerosol changes with time, e.g. by changes in the gas-particle partitioning or due to aging processes, the ratio between different isomers or the educts for thermal decomposition will change causing similar features in single ion thermograms of FIGAERO-CIMS data.

Preliminary tests with a dataset of ambient FIGAERO-CIMS measurements show how PMF immediately separates
the data by its ambient sources (i.e., which precursors and/or processes created the aerosol) and/or SOA type (e.g. fresh
and aged OA). This information is also accessible with a PMF analysis of the time series of mass spectra integrated for
each desorption cycle. However, in addition to this, PMF of the thermal desorption data provides detailed information
on the volatility of each of these sources or SOA types while also showing how much of the signal is affected by thermal
decomposition. This information on the contribution of thermal decomposition is crucial when the FIGAERO-CIMS
data is used to identify the detailed composition or volatility of SOA particles. Details of this investigation will be the
content of a future publication.

4: The highOC/wet case that you're using as evidence for aqueous chemistry is a particular case, in that the aerosol you're producing using the OFR is highly oxidized, and that oxidation happened much faster (and possibly through differing chemical pathways) than would happen in the real atmosphere. Thus, the specific molecules that comprise the aerosol are probably not representative of anything you'd get in the atmosphere. So, while the wet cases for lowOC and mediumOC illustrate that the diffusion limitation to evaporation is decreased in aqueous aerosol, you are suggesting that aqueous chemistry doesn't happen much except for the highOC aerosol, which may no longer be relevant for the atmosphere. Can you add some discussion of how your results relate to atmospheric aerosol?

The highOC SOA in our study is definitively an extreme case. We suggested that many of the compounds affected by aqueous phase chemistry could be organic (hydro)peroxides or contain other functional groups which easily hydrolyse and then continue to react (Buchholz et al., 2019). The (hydro)peroxide formation is probably enhanced by the very high HOx levels in the OFR. But such compounds are not unique to OFR reactors. One formation path of compounds containing several hydroperoxyl or peroxiacid groups may be auto-oxidation of terpenes in the gas-phase which leads to highly oxygenated material (HOM) (Bianchi et al., 2019; Ehn et al., 2014). These compounds play an important role in particle growth and are

being detected more and more in ambient measurements (Lee et al., 2018; Mohr et al., 2017). Another compound class which is possibly susceptible to hydrolysis is organo-nitrates (which did not occur in our study due to the experiment design). Thus,

190   we conclude that ambient aerosol will probably not show as clear signs of aqueous phase chemistry as the high OC case, but to some degree it is very likely and may be detected with the right measurement and analysis method. We mention how (hydro-)peroxides are most likely responsible for the different behaviour of the highOC samples in section 3.3 and extended the conclusion section with regard to the atmospheric relevance.

First paragraph in section 3.3:

195   As discussed by Buchholz et al. (2019), the different behaviour of the highOC SOA is most likely due to higher fractions of (hydro-)peroxides in the particles caused by the much higher HO_2 concentrations in the OFR at the highOC oxidation conditions. Most peroxides are sensitive to hydrolysis which will initiate a range of reactions in the aqueous phase. The low volatility products of these reactions thermally decompose to similar fragments as did the peroxide precursor. Thus, the same groups of ions are detected but at a higher T_{desorp}.

200

Conclusions:

The highOC SOA in our study may not be representative of ambient SOA of the same OC ratio as it was formed under extremely strong oxidation conditions in an OFR. But the type of compounds affected by aqueous phase chemistry (i.e., organic compounds containing (hydro)peroxides or other functional groups which easily hydrolyse and then continue to react) are not

205   unique to OFR reactors. One formation path of compounds containing several hydroperoxyl or peroxiacid groups is the auto-oxidation of terpenes in the gas-phase which leading to highly oxygenated material (HOM) (Bianchi et al., 2019; Ehn et al., 2014). These compounds play an important role in particle growth and are detected more and more in ambient measurements (Lee et al., 2018; Mohr et al., 2017). Another compound class which is possibly susceptible to hydrolysis is organo-nitrates (which did not occur in our study due to the experiment design). Thus, ambient aerosol will probably not show as clear signs

210   of aqueous phase chemistry as the high OC case, but it is very likely that such processes occur to some degree and may be detected with the PMF analysis of FIGAERO thermogram data.

Specific Comments:

Pg. 4 Ln. 9: Which size particles were you selecting in the nano-DMA? Also, it would be useful to mention to flow rates of

215   your sheath and sample flows in the DMA, the ratio of which will determine just how quasi-monodisperse your selected particles become.

The Nano-DMAs were set to select 80 nm particles. The fraction of double charged 120 nm particles was very small (both regarding the total number and mass). Sample flows were always 1.0 lpm and the sheath flows were 10.0 lpm in the dry experiments and 8.0 lpm under wet conditions. The ratio between sheath and sample flow was thus 10 (dry) or 8 (wet) which

220   led to a small increase in broadening in the wet cases.

We have added the information about the particle size in section 2.1 and for the flows in the detailed description in SI section 1.1.

A Nano differential mobility analyser (NanoDMA) was used to select a quasi-monodisperse particle distribution (electromobility diameter 80 nm) …

225 …

The NanoDMA was operated with an open loop sheath flow (10 L min^{-1}, (dry): 8 L min^{-1} (wet)) which together with the extremely short residence time inside the NanoDMA (≤ 0.3 s) limited the diffusion of gaseous compounds into the selected sample flow (1 L min^{-1}).

230 Pg. 4 Ln. 13: You have already assigned the acronym OFR, so you should avoid writing out the words oxidative flow reactor hereafter.

Changed the text as requested.

Pg. 4 Ln. 17: I assume the 0.25 h evap time for fresh particles is due to the collection time on the filter? Please make this clear, 235 as it may confuse readers unfamiliar with FIGAERO operation, and they may wonder why you didn't sample fresh particles without a 15 min delay.

We point this out in the more detailed description in SI section 1.1. but for clarity we highlight this information also in the main manuscript text (page 4 line 22):

Note that the evaporation time of 0.25 h for the "fresh" sample does not stem from residence in the RTC but rather from time 240 needed to collect sufficient mass on the FIGAERO filter (more details in SI section 1.1).

Pg. 11 Ln. 20: Have you considered summing the LB1, LC1 and LC2 factors together? It could be that PMF is splitting up the background factor before pulling out the last of the V-type factors, so you could just recombine the split background factors.

We agree on that the splitting of LC1 and LC2 is probably artificial. But note that the contamination (LC1 and LC2) only 245 occurred for one sample due to "user interference" (most likely some issues when changing the filter or maintaining FIGAERO). Thus, adding LC1 and LC2 to the general background LB1 stemming from the instrument is not helpful.

Pg. 13 Ln. 1: How have you taken into account the effect of the stainless steel RTC walls on changes in VFR? Could there have been different wall effects during dry vs. wet conditions, i.e., different uptake coefficients to the wall surface? When it's 250 humid enough to have one or several monolayers of water molecules on the walls, they could appear very different to a gas or particle than if it's bare metal.

The reviewer is correct in pointing out that "wetted" walls (RTC RH 80%) will have different uptake properties than dry stainless steel.

We tested the capability of the stainless-steel RTC wall to take up all evaporating vapours under dry conditions for a previous study (Yli-Juuti et al., 2017). An increase in SOA mass inside the RTC by a factor of 20 did not change the observed evaporation behaviour. This means that the particle evaporation was not limited by build-up of compounds in the gas phase, i.e., the dry walls acted as "perfect sinks".

Under wet conditions, the changes of wall losses of gases will depend on their Henry's law constants or, more generally, on if the compounds are hydrophilic or hydrophobic. As most of the compounds evaporating from the studied SOA types should be at least slightly hygroscopic, we can expect an increase in wall uptake under wet conditions. As the stainless-steel walls we already such good sinks in the dry case, this increase will not have an effect on the observed evaporation behaviour and composition changes of the particles.

The particle wall loss increases most probably in the wet case as both the walls and the aerosol particles may be more "sticky". Our study is not based on the overall mass conservation. The particle population is homogeneous so loss to the wall reduces the available particulate mass but not the composition of the population.

We have tried to measure the evaporating gaseous compounds with CIMS during some of the evaporation experiments, but the signals were too low for detection. In addition, we did not observe any accumulation of vapours in the gas phase during the evaporation experiments. This confirms that the stainless RTC walls are indeed efficient sink for the vapours.

Table 2: It would be informative if you present here and discuss elsewhere the estimated volatility of each of your V-type factors (by converting their T-max to volatility).

We deliberately did not show the C* values here as we did not want to go into details of the calibration necessary for this conversion. This manuscript is focusing on the method and general interpretation of the PMF factors with regard to the underlying particle phase processes while the companion paper (Tikkanen et al., 2019) investigates how the C* values assigned with this method compare to those derived with process modelling of isothermal evaporation data for the same SOA particles. Assuming an average molecular weight of 200 g mol^{-1} and applying the same T_{max} -> C* calibration as in Tikkanen et al. (2019), we find that the linear part of the FIGAERO heating ramp from 25 °C to 190 °C corresponds to log10(C*) values of +2 to -12. This covers the majority of SVOC to ULVOC (ultra-low volatility organic compounds, Schervish and Donahue, 2020) that can be expected from α-pinene oxidation. We use these C* values to indicate the desorption temperature ranges for S-, L-, and ELVOC in Figures 5 - 7 and S 4 – S 6 as a rough guideline for the reader.

Figure 9: Could you subtract the background signals from the total, such that the V-type factors will add up to the light blue lines? It could be visually easier to understand then.

We changed the Figure as requested. We noticed a small mistake in panel (c) in the original Figure (the reconstructed signal had been used instead of the measured) and a typo regarding the sum formula in the labels of panels (a) and (b) and the corresponding text ($[C_8H_{12}O_5+ I]^-$ is shown, not $[C_8H_{10}O_5 + I]^-$).

References

Bianchi, F., Kurtén, T., Riva, M., Mohr, C., Rissanen, M. P., Roldin, P., Berndt, T., Crounse, J. D., Wennberg, P. O., Mentel, T. F., Wildt, J., Junninen, H., Jokinen, T., Kulmala, M., Worsnop, D. R., Thornton, J. A., Donahue, N., Kjaergaard, H. G. and Ehn, M.: Highly Oxygenated Organic Molecules (HOM) from Gas-Phase Autoxidation Involving Peroxy Radicals: A Key Contributor to Atmospheric Aerosol, Chem. Rev., 119(6), 3472–3509, doi:10.1021/acs.chemrev.8b00395, 2019.

Buchholz, A., Lambe, A. T., Ylisirniö, A., Li, Z., Tikkanen, O.-P., Faiola, C., Kari, E., Hao, L., Luoma, O., Huang, W., Mohr, C., Worsnop, D. R., Nizkorodov, S. A., Yli-Juuti, T., Schobesberger, S. and Virtanen, A.: Insights into the O:C dependent mechanisms controlling the evaporation of a-pinene secondary organic aerosol particles, Atmos. Chem. Phys. Discuss., 1–21, doi:10.5194/acp-2018-1305, 2019.

DeRieux, W.-S. W., Li, Y., Lin, P., Laskin, J., Laskin, A., Bertram, A. K., Nizkorodov, S. A. and Shiraiwa, M.: Predicting the glass transition temperature and viscosity of secondary organic material using molecular composition, Atmos. Chem. Phys., 18(9), 6331–6351, doi:10.5194/acp-18-6331-2018, 2018.

Ehn, M., Thornton, J. A., Kleist, E., Sipilä, M., Junninen, H., Pullinen, I., Springer, M., Rubach, F., Tillmann, R., Lee, B., Lopez-Hilfiker, F., Andres, S., Acir, I. H., Rissanen, M., Jokinen, T., Schobesberger, S., Kangasluoma, J., Kontkanen, J., Nieminen, T., Kurtén, T., Nielsen, L. B., Jørgensen, S., Kjaergaard, H. G., Canagaratna, M., Maso, M. D., Berndt, T., Petäjä, T., Wahner, A., Kerminen, V. M., Kulmala, M., Worsnop, D. R., Wildt, J. and Mentel, T. F.: A large source of low-volatility secondary organic aerosol, Nature, 506(7489), 476–479, doi:10.1038/nature13032, 2014.

Lee, B. H., Lopez-Hilfiker, F. D., D'Ambro, E. L., Zhou, P., Boy, M., Petäjä, T., Hao, L., Virtanen, A. and Thornton, J. A.: Semi-volatile and highly oxygenated gaseous and particulate organic compounds observed above a boreal forest canopy, Atmos. Chem. Phys., 18(15), 11547–11562, doi:10.5194/acp-18-11547-2018, 2018.

Li, Y., Pöschl, U. and Shiraiwa, M.: Molecular corridors and parameterizations of volatility in the chemical evolution of organic aerosols, Atmos. Chem. Phys., 16(5), 3327–3344, doi:10.5194/acp-16-3327-2016, 2016.

Mohr, C., Lopez-Hilfiker, F. D., Yli-Juuti, T., Heitto, A., Lutz, A., Hallquist, M., D'Ambro, E. L., Rissanen, M. P., Hao, L., Schobesberger, S., Kulmala, M., Mauldin, R. L., Makkonen, U., Sipilä, M., Petäjä, T. and Thornton, J. A.: Ambient observations of dimers from terpene oxidation in the gas phase: Implications for new particle formation and growth, Geophys. Res. Lett., 44(6), 2958–2966, doi:10.1002/2017GL072718, 2017.

Schervish, M. and Donahue, N. M.: Peroxy radical chemistry and the volatility basis set, Atmos. Chem. Phys., 20(2), 1183–1199, doi:10.5194/acp-20-1183-2020, 2020.

Schobesberger, S., D'Ambro, E. L., Lopez-Hilfiker, F. D., Mohr, C. and Thornton, J. A.: A model framework to retrieve thermodynamic and kinetic properties of organic aerosol from composition-resolved thermal desorption measurements, Atmos. Chem. Phys., 18(20), 14757–14785, doi:10.5194/acp-18-14757-2018, 2018.

Tikkanen, O., Buchholz, A., Ylisirniö, A., Schobesberger, S. and Virtanen, A.: Comparing SOA volatility distributions derived from isothermal SOA particle evaporation data and FIGAERO-CIMS measurements, Atmos. Chem. Phys. Discuss., (November), 1–34, doi:10.5194/acp-2019-927, 2019.

Yli-Juuti, T., Pajunoja, A., Tikkanen, O. P., Buchholz, A., Faiola, C., Väisänen, O., Hao, L., Kari, E., Peräkylä, O., Garmash, O., Shiraiwa, M., Ehn, M., Lehtinen, K. and Virtanen, A.: Factors controlling the evaporation of secondary organic aerosol from a-pinene ozonolysis, Geophys. Res. Lett., 44(5), 2562–2570, doi:10.1002/2016GL072364, 2017.

320

Reply to Reviewer #3

We thank the Reviewer for carefully reviewing our manuscript and providing insightful comments. Below we address each comment point by point. For clarity we mark the reviewer comment in **blue**, our answers in **black**, and changes to the

5 manuscript in **red**. Page and line numbers in our replies refer to the revised manuscript.

In this work, Buchholz et al. demonstrated for the first time the application of positive matrix factorization (PMF) on high-resolution FIGAERO-CIMS data. They were able to identify distinct volatility classes, background, and decomposition products as PMF factors. Their results also offer additional confirmation of the effects of aerosol water on partitioning and

10 particle-phase processes. Overall, the manuscript is well written and the approach described is novel. However, I have some concerns with the PMF design, experimental design, and data interpretation as described below. I would recommend the manuscript for publication in ACP if these comments are addressed.

PMF design and interpretation

15 2.3.1, page 7, line 19-22. The advantage of PMF is that it requires no a priori information. Pre-grouping thermograms based on knowledge about the SOA precursors, extent of aging, and aerosol water content defeats the purpose of using PMF, if not for laboratory sample then certainly for ambient samples. The advancement brought by the FIGAERO thermogram PMF in its current state is perhaps overstated. This limitation should be discussed in the manuscript. The analysis could also be carried out further to involve different SOA types all at once to validate its usefulness in a broader context.

20 This is the first study applying PMF analysis to FIGAERO-CIMS thermal desorption data. We had to prove that the splitting of single ion thermograms into multiple factors, especially at higher desorption temperatures, was not simply a mathematical construct to reduce Q/Qexp by just adding more factors. With the information about the prior isothermal evaporation (i.e. having samples where the volatile fraction of the particles was removed) we verified that with the removal of the more volatile fraction of the aerosol we removed the low temperature factors whereas the ones formerly explaining the "tail" of the single

25 ion thermograms remained (as shown for three examples in Figure 8).

When applying PMF to a data set of FIGAERO-CIMS thermal desorption data (here all OC cases or generally, ambient data), there were two driving forces for the grouping of compounds into factors: their volatility and their "source" in the atmosphere/chamber/OFR (biomass burning, oxidation of different precursors, day-time/night-time chemistry, etc.). As we were more interested in identifying changes in the volatility due to the isothermal evaporation treatment, we decided to remove

30 the influence of the different SOA sources (here the different oxidation regimes in the OFR) from the data set by splitting it into three groups. This was mostly done to highlight the particle phase processes and reduce the number of factors that had to be compared in each case (7 – 9 vs. 13 or more). The lower number of factors in each case also improves the overall clarity of

the manuscript. But pre-grouping the data is not a requirement for using PMF with thermal desorption data. We adjusted the last paragraph of section 2.3.1 to clarify this:

35

When performing PMF with the combined dataset with all available thermogram scans, the large number of factors (13 or more) necessary to explain the observed variability complicated the analysis and interpretation (see case study in SI section 1.4). Thus, the thermogram scans were grouped by SOA type (i.e., t_{evap} = 0.25 h & 4 h particles, dry & wet conditions of one SOA type: four thermogram scans per group). This pre-grouping reduced the number of factors in each group enhancing their

40 interpretability while still enabling a direct investigation of the changes due to the evaporation/humidification for one SOA type. But generally, splitting the data by SOA type or even knowing about such different SOA types/sources in the data is not a requirement for analysing a thermogram dataset with PMF.

The information about using the filter blank data was moved to the description of the treatment of raw data in section 2.2 (page

45 4, line24):

For the PMF analysis, we did not subtract the filter blank measurements but rather added the corresponding filter blank thermograms to the dataset to help with the identification of the background factors, i.e., factors dominated by compounds from the instrument and/or filter background (more details on factor identification in section 3.1).

50 We strengthen this argument with the case study now provided in SI section 1.4 (see comment below) which concludes with:
This case study shows that the same overall conclusions can be drawn by pre-grouping the data according to the information of the sampling conditions (here the SOA type) or the combined dataset. With the combined dataset a higher number of factors (here at least 13) has to be chosen to cover all details in the dataset equally well. For ambient data a combined, dataset approach is favourable as limited information is available for any pre-grouping and such an extra step is not desirable. For a detailed

55 study on e.g. particle phase processes with designed SOA types (as presented in this study), a pre-grouping can be beneficial to highlight the fine details hidden in the dataset.

We elaborate on comparing the different SOA types/running PMF on combined data sets in the reply to the next two comments and added two new section about this to the SI material (section 1.3 and 1.4).

60

3.1. Page 11, Line 10-13: Why is not a consistent factor identified across all SOA types (L, M, H, x dry, humid)? Is it expected that, for example, species that make up LV1 have negligible contributions to the overall SOA mass and evaporation behavior under the MediumOC ("M") conditions? It seems to me that there is significant factor blending here. Have the authors tried to combine the different SOA types (e.g. L and M) and see if the different factors (e.g. LV1, LV2, MV1, MV2) can be retrieved

65 all the same?

We have combined different SOA types at the same sampling condition for PMF analysis. We present this investigation in the new SI section 1.4 and the summarised conclusions are presented in the reply to the next comment.

This and the previous comment require a more detailed explanation of the performance of PMF for datasets with two different driving forces for the grouping into factors (here SOA type and volatility). As this explanation is also of interest to the future readers of our manuscript, we decided to add two new sections to the SI material. The SI sections are referred to in the manuscript in section 3.1 after the V-type factors are described (page 11 line 20). In SI section 1.3 (also see below) we use an artificial data set to inspect the way in which PMF groups compounds of the same volatility but with different contribution to the SOA samples. In section SI 1.4, we now present PMF results from a dataset combining all three SOA types (low-, medium-, and highOC) for one sampling condition (dry, t_{evap} = 4h). This sampling condition was chosen to remove the influence of the additional contamination (lowOC, dry, t_{evap} = 0.25h) and wet chemistry (highOC wet samples) which would introduce another 2 - 4 factors in the solution.

Briefly, although there are many ions in common especially for the low- and mediumOC case (as the reviewer also points out), this does not necessarily lead to common factors between the SOA types. The ratios between the ions changes significantly (i.e. a common ion A is associated with a set of compounds in one SOA type and correlates with another set of compounds in the other) as the oxidation chemistry is changed switching from low- to mediumOC SOA forming conditions in the OFR. This change in SOA source will dominate the grouping in PMF for compounds with similar volatility. This is what is meant at the end of the Conclusions by "A careful PMF analysis of the thermogram data will reveal the changes in volatility and the contribution of thermal decomposition to the signal in addition to information about changes in the physical sources of the organic material.".

Combining the different SOA types leads to a number of common factors if an 8-factor solution is selected. However, this solution would not be categorised as "best" according to the criteria used to select the solution for the pre-grouped dataset. A 13-factor solution (which is of the same quality as the ones for the pre-grouped dataset) explains 20-25% of the signal of each SOA type by common factors. All V-type factors from the pre-grouped dataset have a similar counterpart in the 13-factor solution. Thus, we conclude that the pre-grouping is not the main reason for the absence of common factors between the SOA types but caused by the reasons given in the previous paragraph and in more detail in SI section 1.3.

SI section 1.3:

1.3 Drivers controlling the grouping of compounds into PMF factors

When analysing a data set of FIGAERO-CIMS thermal desorption containing multiple samples with PMF, there are two driving forces for the grouping of compounds into factors: their volatility and their "source" in the atmosphere/chamber/OFR

100 (biomass burning, oxidation of different precursors, day-time/night-time chemistry, etc.). To investigate the competition between these two drivers, we create simple artificial data sets (Figure S 10). We combine 4 compounds A, B, C, and D (with nominal ion masses of 1, 2, 3, and 4) to form 4 SOA types (SOA1, SOA2, SOA3, SOA4). A, B, and C have the same volatility. A has the same thermogram in each SOA type.

In scenario X, we investigate as an extreme case the combination of SOA1 (containing A, B, and D) and SOA2 (containing A,
105 C, and D). This scenario can be interpreted one source/process creating A and B at the same time for SOA1, but than a different pathway created A together with C in the case of SOA2. The 3-factor solution PMF result for this scenario (SOA1 & SOA2) is shown in Figure S 11. The common compound A has exactly the same thermogram behaviour in both samples. But as it once correlates with B (in SOA1) and once with C (SOA2), A is explained with Factor 1 (black) for the SOA1 sample and with Factor 2 (red) for the SOA 2 sample. Even increasing the number of factors does not create a "common" factor which
110 contains only A. For this scenario, the different "source" for A (which lead to different compounds correlating with it) dominates the factor identification and not the fact that A, B, and C have the same volatility. Note that compound D which also does not change between SOA1 and SOA2 is separated into its own factor. Here the difference in volatility (from A, B, and C) is the driving force for the factor grouping.

In scenario Z, SOA3 and SOA4 each contain all 4 compounds. The concentration of A is the same in both types while the
115 contribution of C is higher in SOA4 than in SOA3 and that of B is lower. The 3-factor solution for this scenario is depicted in Figure S 12. Again, we find two factors explaining the behaviour of the three compounds with the same volatility. But now factor 2 (red, dominated by A and C) has a considerable contribution to both SOA types. Figure S 13 shows how the thermograms of A are explained by the two factors. Similar to scenario X, we can interpret the factor grouping by changes in the processes/sources producing the compound A, B, and C. Factor 1 (black) stands for process 1 creating the majority of C
120 and some A. Process 2 creates mostly A and B is explained by factor 2. Again factor 3 (containing D) is again differentiated by the different volatility of D. Integrating the factor thermogram profiles shows that the more volatile fraction of SOA4 is formed by process 2 while that the fraction of SOA3 with the same volatility is formed by both processes 1 and 2 (Figure S 14).

This Scenario Z is very similar to comparing e.g. samples from low- and mediumOC SOA. Many ions occur in both SOA
125 types, but the ratios between them change. Many products in the oxidation of α-pinene can be formed via different pathways, but depending on the reaction path, they will correlate with different other products. The change in the oxidation field (increase of [O_3] and [OH]) probably affected the HO_2/RO_2 chemistry which has a strong influence on e.g. highly oxygenated material (HOM) and dimer formation, i.e. we changed the ratio between reaction paths.

130 SI section 1.4:

1.4 PMF analysis of a dataset combining different SOA types

To study if the different SOA types are really as different as the factors identified in section 3.1 suggest or if this was artificially introduced by pre-grouping the data, we conduct a PMF analysis with the data grouped by sampling conditions. The dry, t = 4 h

4

set was chosen for detailed analysis as we did not want to introduce the added complication of aqueous phase chemistry and the dry lowOC sample at t = 0.25 h had a large contamination unique to that sample. In the following, we will refer to this as the "combined dataset". The analysis conducted with data pre-grouped by the SOA type will be labelled "pre-grouped".

The 8- and 13 factor solutions for the combined dataset are shown in Figure S 15 and Figure S 16. Based on the change in $Ratio_{exp}$ values and the residual time series, 8 was the minimum number of factors need to capture the thermograms of all 3 SOA types equally well. But to reach residuals as low as in the pre-grouped datasets, 13 factors are needed. Especially the lower T_{desorp} regions in the low- and highOC case and the high T_{desorp} part of the mediumOC sample are improved (Figure S 17). Note that with the same criteria applied in the section 2.3.3, we would not select the 8-factor solution as a "best" solution. There are no factors in the 8-factor solution which are unique to one SOA type. 4 factors (FV1, FV4, FV7, and FB/D1) occur in all SOA types explaining 80% of the signal of the mediumOC sample and 50% of the low- and highOC samples. The other 50% of the signal are explained with two factors each (lowOC: FV2 and FV5, highOC: FV3 and FV7) which also occur in the mediumOC sample.

The 8-solution suggests very strong similarities between the three SOA types with a gradual shift in composition with increasing oxidation. But this solution does not capture the detailed thermogram behaviour of single ions very well as the high residuals suggest (Figure S 18 for the example ion also discussed in sections 3.2 and 3.3). When this is improved in the 13-factors solution, the degree of similarity decreases. Here, 20% - 25% of the signal in each SOA type is explained by factors common to all SOA types (FD1, FB1, and FV1). There are some factors with significant contribution to two SOA types (e.g. FV2 and FV10 for low-/mediumOC or FV3, FV6 and FV11 for medium-/highOC).

To compare the factor mass spectra derived with the combined and the pre-grouped datasets, we use the spectral contrast angle, θ. θ is derived from the dot product of two mass spectra (Wan et al., 2002):

$$cos\theta = \frac{\sum_i a_i b_i}{\sqrt{\sum_i a_i^2 \cdot \sum_i b_i^2}}$$

where a_i and b_i are the intensities of ion i in mass spectrum 1 and mass spectrum 2. Two mass spectra are considered to be similar if θ is between 0° and 15°, somewhat similar but with important differences if θ is between 15° and 30°, and different with θ values >30° (Bougiatioti et al., 2014).

The results from the pairwise comparison of each factor identified in the pre-grouped datasets with all factors from the combined dataset are shown in Figure S 19. All V-type factors identified in the pre-grouped dataset have a (at least somewhat) similar counterpart in the combined dataset (e.g. LV4 and FV7, MV4 and FV8, HV2 and FV6). This shows that the missing similarities between factors identified in the pre-grouped dataset is not artificially induced by the pre-grouping but rather stems from the shifts in SOA composition with increasing oxidation. The changes in the groups of correlating ions will cause compounds that occur in all SOA types to be grouped into different factors as explained with the simplified dataset in SI section 1.3. The factors FV2, FV3, and FV4 show similarities to two factors within the corresponding SOA types. This suggests that either more factors are needed in the combined dataset to resolve the thermogram behaviour of the compounds represented by these factors, or that there was "factor-splitting" in the pre-grouped dataset (i.e. too many factors). Also, the combined

5

dataset uses only the information from the dry, $t_{evap} = 4$ h sample while the pre-grouped ones contain all 4 sampling types. Thus, behaviour unique to a different sample type cannot be correctly captured (e.g. LC1&2 or H-WET).

This case study shows that the same overall conclusions can be drawn by using pre-grouping the data according to the information of the sampling conditions (here the SOA type) or the combined dataset. With the combined dataset a higher number of factors (here at least 13) has to be chosen to cover all details in the dataset equally well. For ambient data a combined, dataset approach is favourable as limited information is available for any pre-grouping and such an extra step is not desirable. For a detailed study on e.g. particle phase processes with designed SOA types (as presented in this study), a pre-grouping can be beneficial to highlight the fine details hidden in the dataset.

Experimental Design

SI 1.1: Some experimental designs are unclear. Did the collection of the 0.25 hr isothermal evaporation sample start immediately after filling up after size selection? Was the t_0.25hr aerosol collected directly at the outlet of the DMA column, or was the aerosol drawn through the RTC first?

The $t_{evap} = 0.25$h sample was collected directly from the outlet of the Nano-DMAs and the residence time is the average time particles resided on the filter between their collection and the start of the desorption. The 15 min residence time for "fresh" particles and its consequences is explained in the last paragraph of SI section 1.1. We have included this information now in the short description in the main manuscript and modified the passage in SI section 1.1 to make this clearer:

Main text:

Note that the evaporation time of 0.25 h for the "fresh" sample does not stem from residence in the RTC but rather from the collection time on the filter (see SI section 1.1 for details). Due to this minimum evaporation time the FIGAERO-CIMS measurements will underestimate the contribution of volatile compounds in the particles as they leave the OFR.

SI section 1.1:

Two types of particles samples were collected with the FIGAERO-CIMS: "fresh" particles (labelled $t_{evap} = 0.25$h) were collected directly after size selection with a nano differential mobility analyser (NanoDMA, 80 nm electro mobility size) and "RTC" particles (labelled $t_{evap} = 4$h) which were left to evaporate at ~20 °C for 3 - 4 h in a residence time chamber (RTC) prior to collection on the FIGAERO filter.

Evaporation of aerosol already collected on the filter during the 15 minute collection period is likely to be significant for t_0.25hr samples, and should therefore be taken into account. It would be good to show, at least qualitatively, how much effects this has for different evaporation timescales.

The collection period was 30 min for the fresh samples. 15 min is the average time the particles reside on the filter before the desorption starts. From the isothermal evaporation experiments we know that between 4% (highOC, dry) and 32% (lowOC,

6

wet) of the particle volume evaporates in the first 15 min. This information was used when comparing the contribution of V-type factors in Figure 8. The x-axis position of the bars is the average VFR value from the isothermal evaporation

205 Considering the potential artifacts introduced by the use of a stainless RTC (as mentioned by the other referee), I was surprised that the authors did not attempt (or mention) isothermal evaporation directly over the FIGAERO filter, as has been done in some previous studies (e.g. Schobesberger et al. 2018). It seems to me a lost opportunity to monitor gas-phase changes that can corroborate particle-phase observations. I would like to see a comparison between isothermal evaporation RTC vs. FIGAERO filter results, at least under dry condition, that shows if there is any systematic biases introduced by the use of RTC. Such a direct comparison of these two methods would indeed be very interesting. Please, note that our experiments were

210 conducted in 2016 while the earliest publications about FIGAERO-filter evaporation studies came out in 2018 (D'Ambro et al., 2018). Later, we did discussed our results with scientist involved in the FIGAERO-filter evaporation studies. Direct comparisons of the methods are difficult as different FIGAERO and chamber design were used. However, qualitatively we observe very similar behaviour, namely the removal of the signal fraction at lower Tdesorp values leading to more shallow and broader single ion thermograms.

215 The original purpose of the experiments creating this data set was to provide reliable and direct measurements of isothermal evaporation as a base for detailed process modelling (Buchholz et al., 2019; Yli-Juuti et al., 2017). The particle size measurements during isothermal evaporation in the RTC is not biased by any assumptions about mass conservation/wall losses/filter collection issues. The FIGAERO-CIMS measurements were added to quantify chemical composition changes during this isothermal evaporation as the Aerosol Mass Spectrometer (AMS, Aerodyne Research Inc.) could not reliably detect

220 the expected changes.

The potential artefacts of stainless-steel walls are mostly concerning reactions on those walls (e.g. peroxide decomposition as mentioned by reviewer #2) or increased uptake of oxygenated compounds from the gas phase. In our setup, all compounds that evaporate from the particles are considered lost to the walls and not interfering with the particles anymore. Tests with different aerosol loadings in the RTC showed no significant differences in particle evaporation. This confirms that the stainless-

225 steel walls are very effective in taking up the evaporated compounds and there is no build-up of compounds in the gas phase. We are collecting and investigating the remaining particles after isothermal evaporation in the RTC and determine their composition. This composition is representative for the residual particles after isothermal evaporation independent on how many particles were lost to the walls and what happened to the evaporated vapours once they were taken up by the walls.

With the FIGAERO-filter evaporation method different types of possible artefacts have to be considered, e.g. differences in

230 mass loading on the filter can shift T_{max} values considerably (SI material to Huang et al., 2018). These can be avoided with the RTC based approach presented here.

235 Minor comments

Figure S5: Were the labels for MV1 and MV2 switched? It is also surprising that the Tmax increases going from ELVOC, LVOC, to SVOC categories, if the labels are indeed correct.

Yes, the labels M1 and M2 were indeed switched in Figure S5. We corrected this. Note that the labels were correct in Figure 6 in the main manuscript.

240

Page 2. Line 5: The application of this technique to ambient data is not shown or discussed in the manuscript. This sentence should be removed.

We simply want to point out that the presented method is not restricted to lab data sets. We are currently studying the application of this method to an ambient data set which will be the content of a future publication.

245

Page 2. Line 6: What is meant by "physical source"?

We were referring to the typical "sources" identified with PMF analysis of e.g. AMS data. There factors are interpreted as organic aerosol (OA) types such as hydrocarbon-like (HOA) or oxygenated OA (OOA). Another way of interpretation is linking the time series of factors to other measurements identifying the process forming the OA (e.g. traffic emissions). We

250 clarified this in the text:

There, it adds the information about particle volatility to that about the sources (such as biomass burning or oxidation of different precursors) or the type (e.g. hydrocarbon-like (HOA) or oxygenated organic aerosol (OOA)) of the organic aerosol particles which could also be obtained by PMF analysis of the mass spectra data integrated for each thermogram scan.

255 Page 4. Line 7-9: Operational details of the DMA column should be mentioned here.

We prefer to keep the description of the setup as brief as possible as it was already described elsewhere. The details for Nano-DMA operation are now given in SI section 1.1.

The NanoDMA was operated with an open loop sheath flow (10 L min^{-1}, (dry): 8 L min^{-1} (wet)) which together with the extremely short residence time inside the NanoDMA (≤ 0.3 s) limited the diffusion of gaseous compounds into the selected

260 sample flow (1 L min^{-1}).

Page 4. Line 9-11: Potential artifacts related to the use of stateliness steel chamber, e.g. peroxide decomposition, should be mentioned.

The system is not operated in a partitioning equilibrium, but rather so that all evaporating vapours are quickly lost to the walls

265 as shown in (Yli-Juuti et al., 2017). Thus, it does not matter if a peroxide that evaporated from a particle decomposes on the RTC wall as long as the decomposition products are not released back into the gas phase and interact with the particles.

Page 7. Line 2-3: What is the reason for using the absolute value instead of the squared value?

When using the squared values with our data, the sum of $Var_{explained}$ and $Var_{unexplained}$ was not equal to Var_{total} but much smaller
270   for PMF solutions with low factor number and larger for solutions with higher factor numbers. This led to Ratio$_{exp}$ >1 which were not meaningful in this context. Also, if the calculation was performed in the other dimension, i.e., calculating the variance with respect to the average value for each observation j instead of the average for each ion i, the values for $Var_{explained}$ / Var_{total} changed.

When using the absolute distances instead of the quadratic this behaviour changed and $Var_{explained} + Var_{unexplained} \approx Var_{total}$. Thus,
275   we decided to use this metric as a compromise.

Page 9, Line 27-29: Please remove the "great"s.
Text was changed.

280   Page 10, Line 4: Ulbrich et al., 2009 has already shown that the change in Q/Qexp with respect to the number of factor is a more reliable indicator than Q/Qexp. This is mentioned later in this manuscript, but should perhaps be moved up to this section here.
Yes, the reviewer is correct. We have actually pointed this out in our original submission (page 10, line 17):
"However, the shape of the Q/Q_{exp} vs number of factors curve can be used to judge the impact of introducing another factor,
285   i.e., a large change in Q/Q_{exp} suggests the new factor explains a large fraction of the variability in the data (Ulbrich et al., 2009)."

Page 10, Line 13-16: Maybe a quotient could be defined here, such as the incremental increase in ion behaviors well-captured (what is the criteria for "well-captured"?) vs. number of factors chosen. What is correlation of the two for the PMF solutions
290   obtained here?
One difficult issue is the fact that the typical parameters to judge the quality of a PMF solution (like Q/Qexp or explained variance) did not provide insights regarding these specific ions and if their characteristic behaviour was captured. As these metrics are all summed over all ions and/or observations they are apparently not sensitive. It was in each case only a few ions where the behaviour was obviously not captured. These ions were all classified as "strong" (i.e., good signal-to-noise ratio).
295   But compared to the large number of other ions, they seem to not have a big enough impact on things like Q/Qexp or explained variance. The most robust way was to inspect the residuals as time series and mass spectra to identify time periods and ions that were not treated adequately.

Page 11, Line 17-19: Table 1 would suggest that background ions were dominated by organic residues instead of fluorinated
300   compounds. Which is the case here?
Fluorinated compounds were identified in the samples but accounted for less than 1% of the total signal. The average F content for V-type factors was < 0.01 and higher for B-, C-, and D-type factors (0.01 – 0.05). The small increase shows that there was

a contribution of "Teflon" compounds to the background, but the majority of the B factor compounds are indeed residual compounds and/or contaminations during sampling.

305 As the contribution of fluorine to the average compositions was so small, it was omitted in Table 1 in the manuscript.

Figures

The figures are the same as were added to the SI material. Thus, we use the same labels and numbering here.
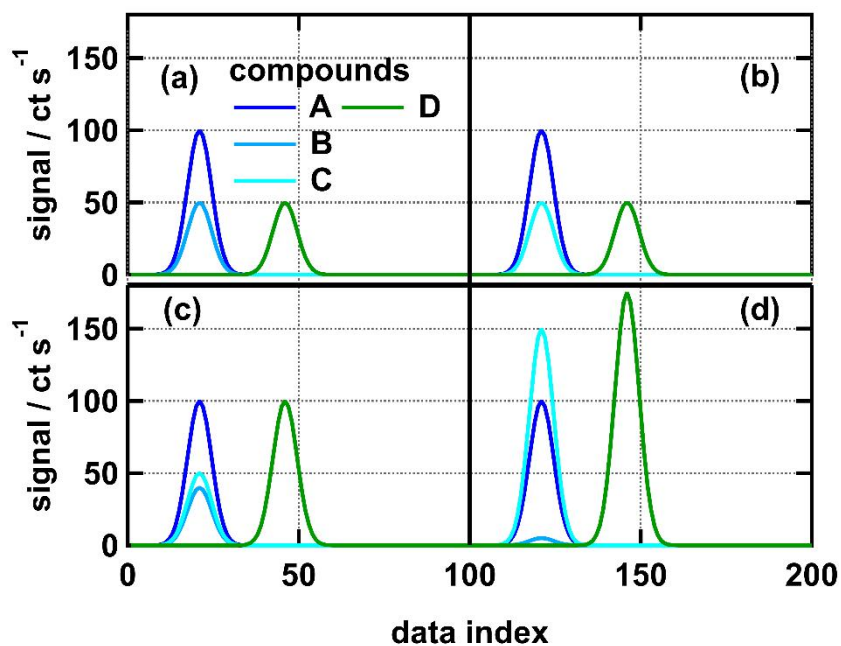
310 **Figure S 10:** Artificial thermogram data for four SOA types. (a) SOA1, (b) SOA2, (c) SOA3, (d) SOA4. SOA1 and SOA2 are combined in one data set for scenario X and so are SOA3 and SOA4 for scenario Z. Note that the thermograms are plotted vs data index. Compounds A, B, and C have the same T_{max} values in all SOA types.
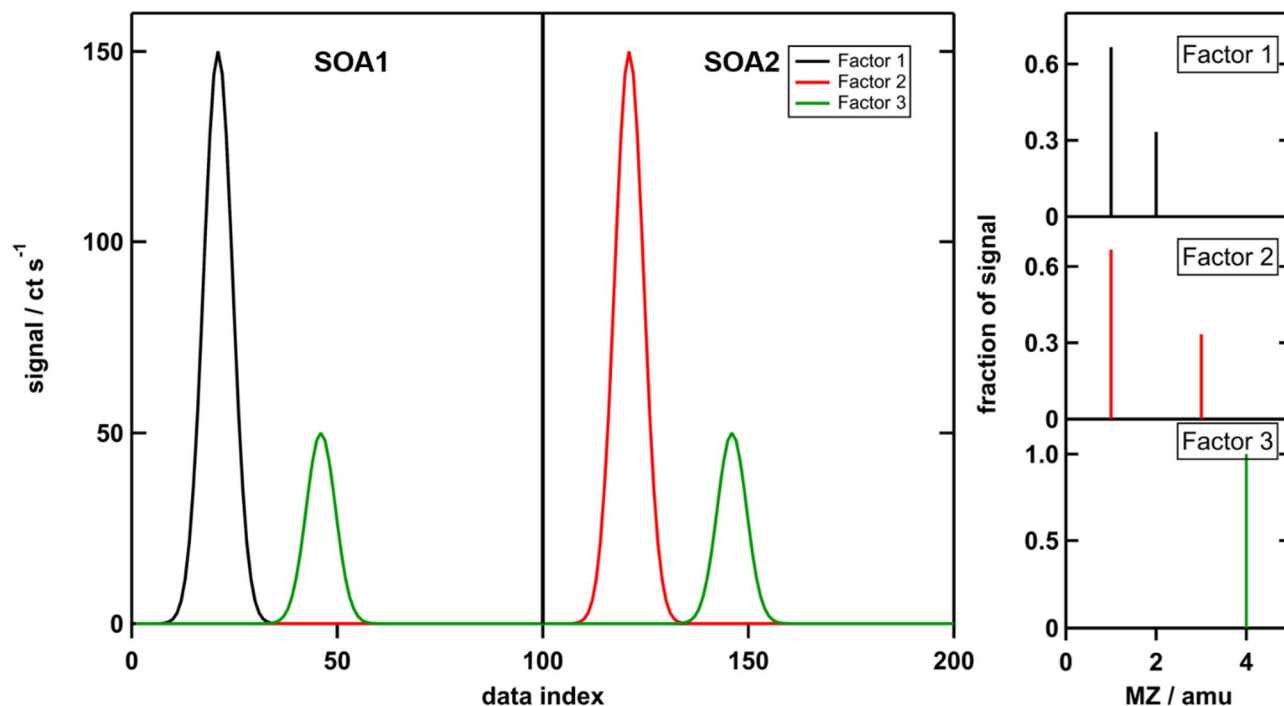
Figure S 11: Factor thermogram profiles (left) and factor mass spectra (right) for the 3-factor solution for scenario X. For plotting, the compounds A, B, C, D are assigned the nominal MZ values 1, 2, 3, 4 respectively.
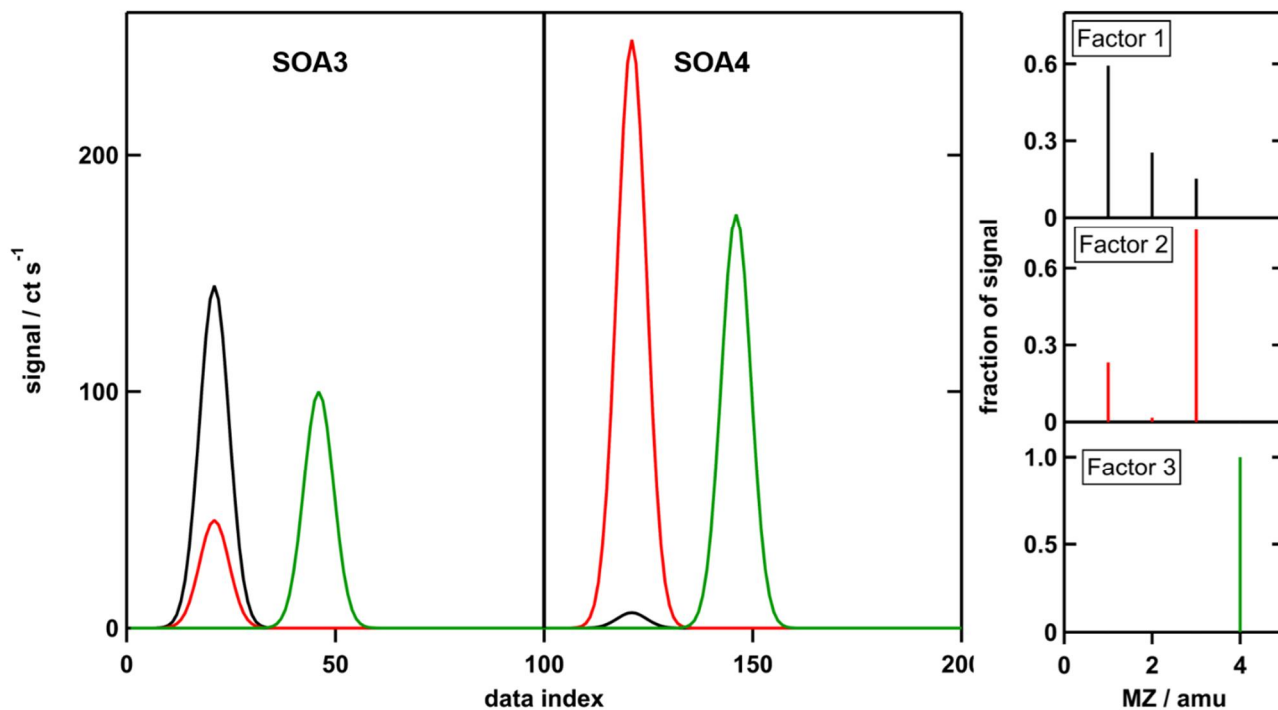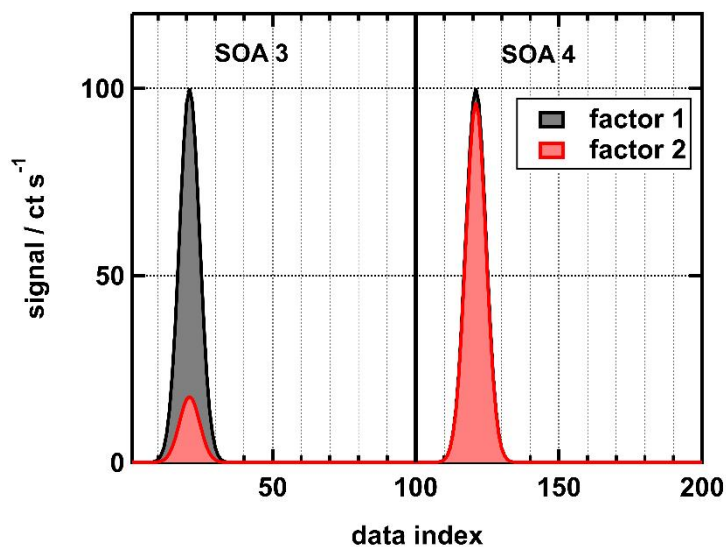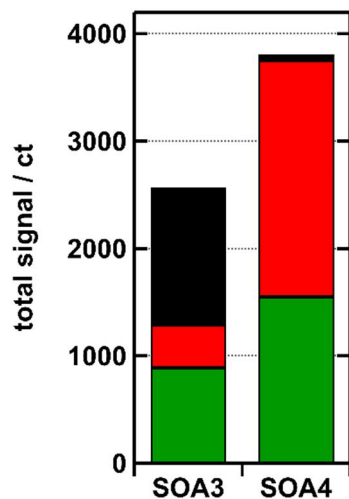
Figure S 12: Factor thermogram profiles (left) and factor mass spectra (right) for the 3-factor solution for scenario Z. For plotting, the compounds A, B, C, D are assigned the nominal MZ values 1, 2, 3, 4 respectively.

320

Figure S 13: Factor thermogram for compound A in scenario Z.

Figure S 14: Absolute contribution of factors to the signal of SOA3 and SOA4 in the scenario Z. Black: factor 1, red: factor 2, green: factor 3.
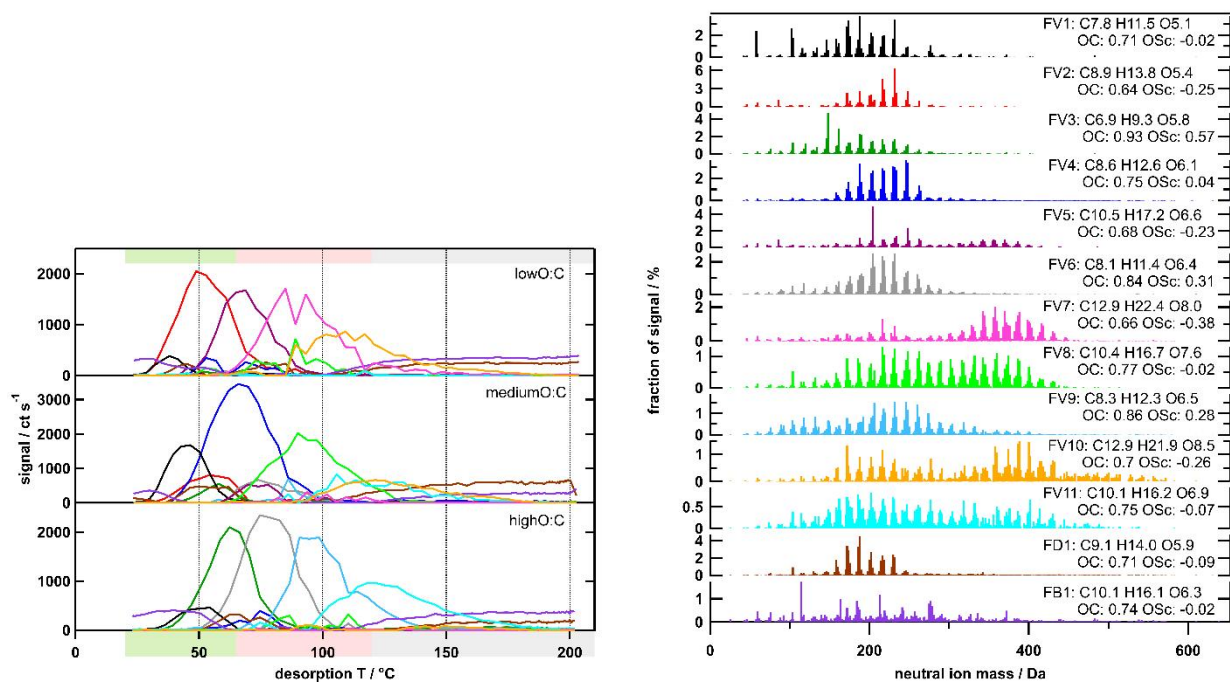

325
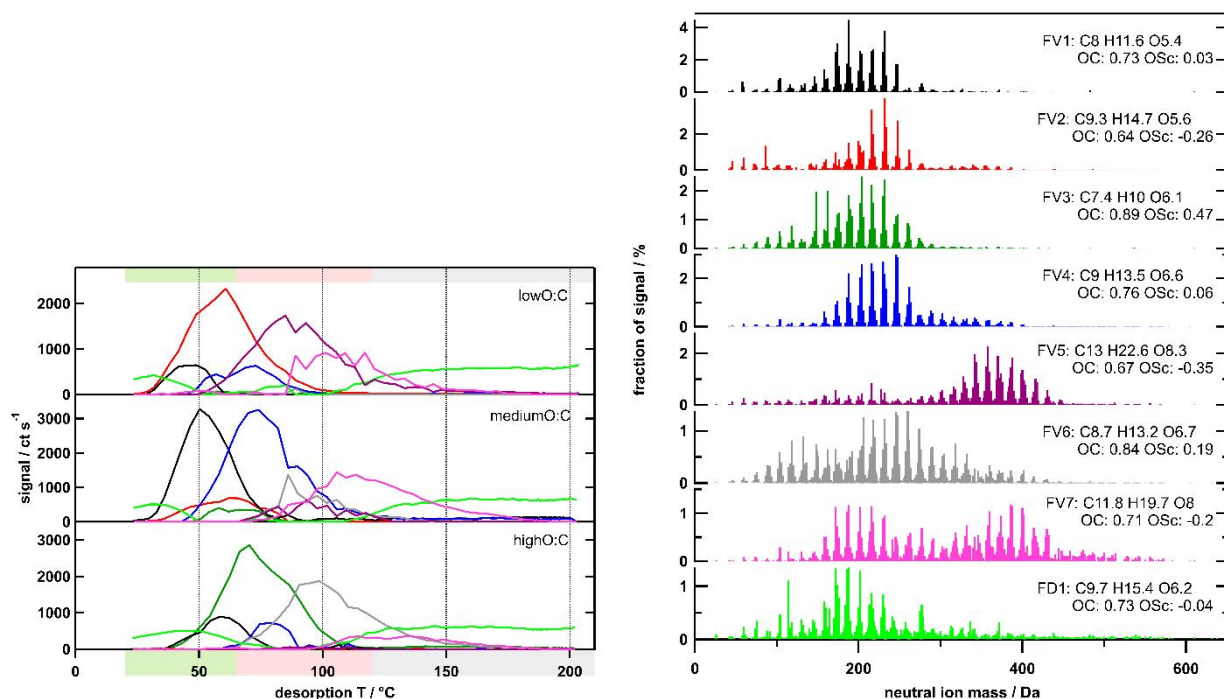
Figure S 15: Temperature profiles (left) and factor mass spectra (right) for the 8-factor solution the combined dataset for dry, t = 4 h samples. Each factor mass spectrum is normalised. The colour code is the same for both panels. Background colour in the left panel indicates volatility classification derived from T_{max}-C* calibrations (green: SVOC, red: LVOC, grey: ELVOC).

13

330

Figure S 16 Temperature profiles (left) and factor mass spectra (right) for the 8-factor solution the combined dataset for dry, t = 4 h samples. Each factor mass spectrum is normalised. The colour code is the same for both panels. Background colour in the left panel indicates volatility classification derived from Tmax-C* calibrations (green: SVOC, red: LVOC, grey: ELVOC).

14
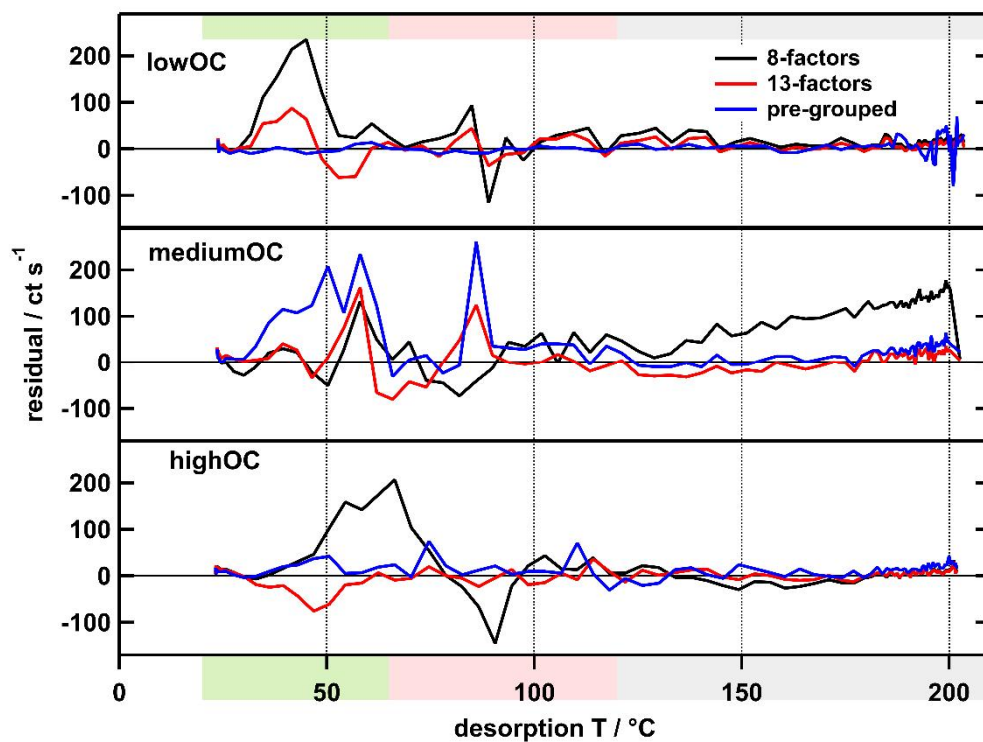
335 **Figure S 17** Time series of residuals for the 8-(black) and 13- factor (red) solutions for the combined dataset and the corresponding pre-grouped datasets (blue).
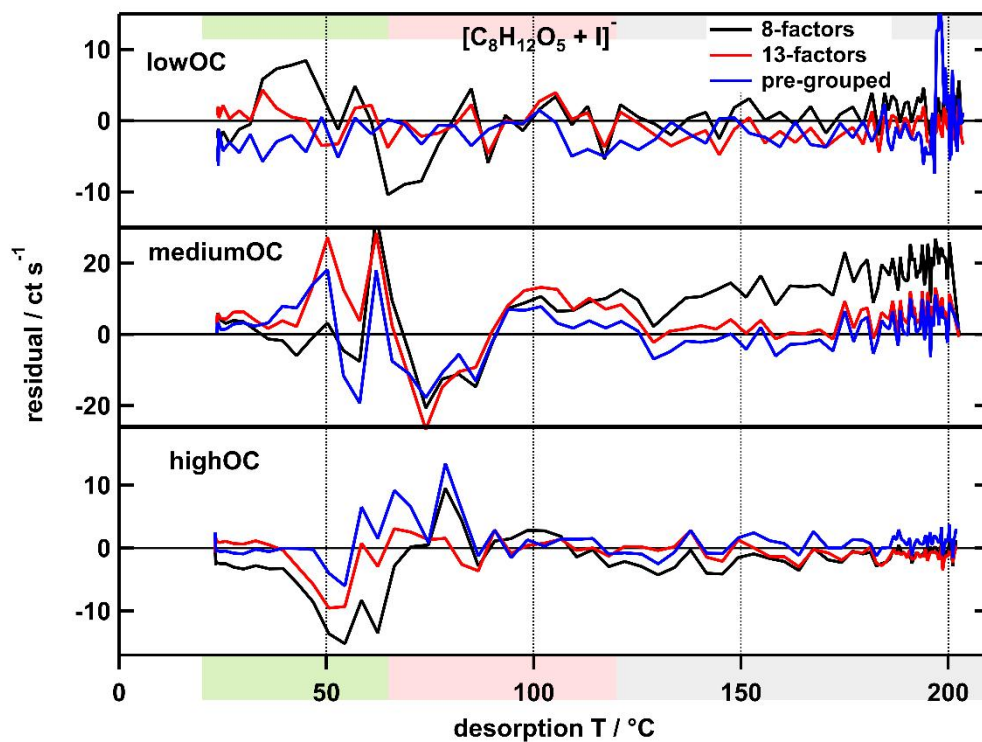
Figure S18: Time series of residuals of the ion $[C_8H_{12}O_5 + I]^-$ for the 8-(black) and 13- factor (red) solutions for the combined dataset and the corresponding pre-grouped datasets (blue).
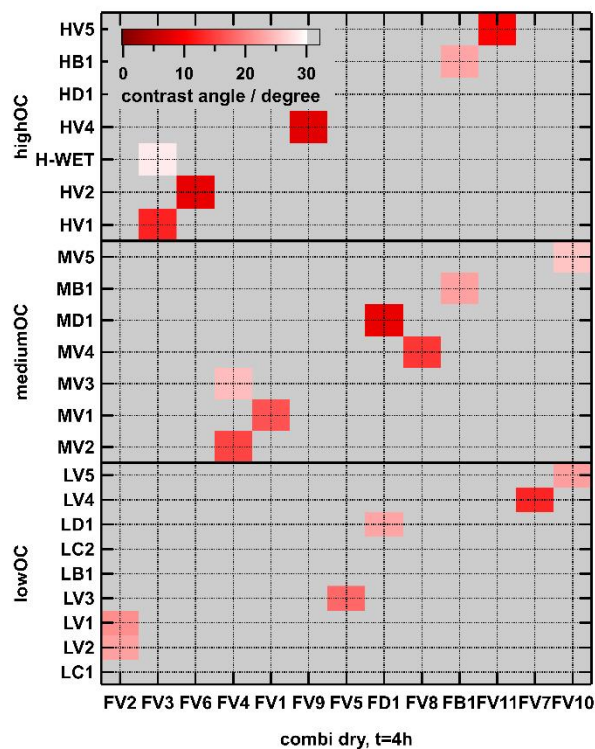
340

16

Figure S 19: Contrast angle plot comparing the factor mass spectra from the separate PMF analysis of each SOA type with those from the combined analysis with 13 factors. Grey areas indicate no similarity (contrast angle > 30°) while shapes of red indicate decreasing degree of similarity from dark to light.

References

350   Bougiatioti, A., Stavroulas, I., Kostenidou, E., Zarmpas, P., Theodosi, C., Kouvarakis, G., Canonaco, F., Prévôt, A.S.H., Nenes, A., Pandis, S.N., Mihalopoulos, N., 2014. Processing of biomass-burning aerosol in the eastern Mediterranean during summertime. Atmos. Chem. Phys. 14, 4793–4807. https://doi.org/10.5194/acp-14-4793-2014

Buchholz, A., Lambe, A.T., Ylisirniö, A., Li, Z., Tikkanen, O.-P., Faiola, C., Kari, E., Hao, L., Luoma, O., Huang, W., Mohr, C., Worsnop, D.R., Nizkorodov, S.A., Yli-Juuti, T., Schobesberger, S., Virtanen, A., 2019. Insights into the O:C

355   dependent mechanisms controlling the evaporation of a-pinene secondary organic aerosol particles. Atmos. Chem. Phys. Discuss. 1–21. https://doi.org/10.5194/acp-2018-1305

D'Ambro, E.L., Schobesberger, S., Zaveri, R.A., Shilling, J.E., Lee, B.H., Lopez-Hilfiker, F.D., Mohr, C., Thornton, J.A., 2018. Isothermal Evaporation of α-Pinene Ozonolysis SOA: Volatility, Phase State, and Oligomeric Composition. ACS Earth Sp. Chem. 2, 1058–1067. https://doi.org/10.1021/acsearthspacechem.8b00084

360   Huang, W., Saathoff, H., Pajunoja, A., Shen, X., Naumann, K.-H., Wagner, R., Virtanen, A., Leisner, T., Mohr, C., 2018. α - Pinene secondary organic aerosol at low temperature: chemical composition and implications for particle viscosity. Atmos. Chem. Phys. 18, 2883–2898. https://doi.org/10.5194/acp-18-2883-2018

Ulbrich, I.M., Canagaratna, M.R., Zhang, Q., Worsnop, D.R., Jimenez, J.L., 2009. Interpretation of organic components from Positive Matrix Factorization of aerosol mass spectrometric data. Atmos. Chem. Phys. 9, 2891–2918.

365   https://doi.org/10.5194/acp-9-2891-2009

Wan, K.X., Vidavsky, I., Gross, M.L., 2002. Comparing similar spectra: From similarity index to spectral contrast angle. J. Am. Soc. Mass Spectrom. 13, 85–88. https://doi.org/10.1016/S1044-0305(01)00327-0

Yli-Juuti, T., Pajunoja, A., Tikkanen, O.P., Buchholz, A., Faiola, C., Väisänen, O., Hao, L., Kari, E., Peräkylä, O., Garmash, O., Shiraiwa, M., Ehn, M., Lehtinen, K., Virtanen, A., 2017. Factors controlling the evaporation of secondary organic

370   aerosol from a-pinene ozonolysis. Geophys. Res. Lett. 44, 2562–2570. https://doi.org/10.1002/2016GL072364

Deconvolution of FIGAERO-CIMS thermal desorption profiles using positive matrix factorisation to identify chemical and physical processes during particle evaporation

Angela Buchholz[1], Arttu Ylisirniö[1], Wei Huang[2], Claudia Mohr[3], Manjula Canagaratna[4], Douglas R. Worsnop[4], Siegfried Schobesberger[1], Annele Virtanen[1]

[1]Department of Applied Physics, University of Eastern Finland, Kuopio, Finland
[2]Institute of Meteorology and Climate Research, Karlsruhe Institute of Technology, Karlsruhe, Germany
[3]Department of Environmental Science and Analytical Chemistry, Stockholm University, Stockholm, Sweden
[4]Aerodyne Research Inc., Billerica, MA 08121-3976, USA

Abstract

Measurements of aerosol particles with a filter inlet for gases and aerosols (FIGAERO) together with a chemical ionisation mass spectrometer (CIMS) yield the overall chemical composition of the particle phase. In addition, the thermal desorption profiles obtained for each detected ion composition contain information about the volatility of the detected compounds, an important property to understand many physical properties like gas/particle partitioning. We coupled this thermal desorption method with isothermal evaporation prior to the sample collection to investigate the chemical composition changes during isothermal particle evaporation and particulate water driven chemical reactions in α-pinene SOA of three different oxidative states. The thermal desorption profiles of all detected elemental compositions were then analysed with positive matrix factorisation (PMF) to identify the drivers of the chemical composition changes observed during isothermal evaporation. The key to this analysis was to use the error matrix as a tool to weight the parts of the data carrying most information (i.e., the peak area of each thermogram) and to run PMF on a combined dataset of multiple thermograms from different experiments to enable direct comparison of the individual factors between separate measurements.

PMF was able to identify instrument background factors and separate them from the part of the data containing particle desorption information. Additionally, PMF allowed us to separate the direct desorption of compounds detected at a specific elemental composition from signals at the same composition stemming from thermal decomposition of thermally instable compounds of lower volatility. For each SOA type, 7 – 9 factors were needed to explain the observed thermogram behaviour. The contribution of the factors depended on the prior isothermal evaporation. Decreased contributions from the lowest desorption temperatures factors were observed with increasing isothermal evaporation time. Thus, the factors identified with PMF could be interpreted as volatility classes. The composition changes in the particles due to isothermal

evaporation could be attributed to the removal of volatile factors with very little change in the desorption profiles of the individual factors (i.e., in the respective temperatures of peak desorption, T_{max}). When aqueous phase reactions took place, PMF was able to identify a new factor which directly identified ions affected by the chemical processes.

We conducted PMF analysis of FIGAERO-CIMS thermal desorption data for the first time using laboratory generated SOA particles. But this method can be applied to e.g. ambient FIGAERO-CIMS measurements as well. ~~In addition to the~~ There, it adds the information about particle volatility to that ~~information~~ about the ~~physical~~ sources (such as biomass burning or oxidation of different precursors) or the type (e.g. hydrocarbon-like (HOA) or oxygenated organic aerosol (OOA)) of the organic aerosol particles. While the latter~~which~~ could also be obtained by PMF analysis of the mass spectra data integrated for each thermogram scan, only the analysis of the thermal desorption data can reveal information about volatility and at the same time identify the contribution of thermal decomposition to the overall signal.~~), changes in particle volatility can be investigated.~~

1   Introduction

To understand the impact of secondary organic aerosol (SOA) on the earth's climate and human health, we need to know more about the chemical and physical properties of these particles and how they evolve with time in the atmosphere. The physical properties of SOA particles are controlled by the physical properties of their constituents and the interaction of the compounds in these complex mixtures. Volatility of SOA constituents is one of the defining characteristics of SOA particles as it plays a key role in understanding (and predicting) the partitioning behaviour of a compound between the gas and particle phase (Pankow, 1994a, 1994b; Pankow et al., 2001). Generally, whether a compound partitions into the particle phase is controlled by the saturation vapour pressure (volatility) of the involved compound, its concentrations, and the available condensation sink. In addition to that, particle phase processes also play an important role, especially when particle-phase compounds are partitioning back into the gas phase. In highly viscous or solid particles, mass transfer limitations exist that reduce the apparent particle volatility (Buchholz et al., 2019; Wilson et al., 2015; Yli-Juuti et al., 2017). The partitioning process gets complicated further by particle-phase chemical reactions. Accretion reactions can convert more volatile compounds into larger and heavier compounds thereby again changing the overall properties of the SOA particles (Herrmann, 2003; Kroll and Seinfeld, 2008). Particulate water plays a special role in these particle phase processes. On the one hand, it will act as a plasticiser, reducing the particle viscosity (Renbaum-Wolff et al., 2013; Virtanen et al., 2010) and thus reducing the mass transport limitation in the particles. ~~which~~ These transport limitations are responsible for the reduced evaporation under dry conditions ~~hinders evaporation~~ (Liu et al., 2016; Wilson et al., 2015; Yli-Juuti et al., 2017). On the other hand, the presence of an aqueous phase enables a wide range of chemical reactions with the potential of forming low volatility compounds via oligomerisation reactions (e.g. Surratt et al., 2007; Tolocka et

2

al., 2004). Hydrolysis of labile bonds (e.g. peroxides or esters) is also possible, which would lead to more volatile products.

There are many challenges involved in trying to fully characterise SOA particles and their volatility. Already the sheer number of precursor compounds and their reaction products, which may contribute to the particle phase by forming new particles or condensing on existing ones, makes it almost impossible to fully characterise the chemical composition of SOA particles (Glasius and Goldstein, 2016; Goldstein and Galbally, 2007). However, the development of the filter inlet for gases and aerosols (FIGAERO, Lopez-Hilfiker et al. (2014)) for the chemical ionisation mass spectrometer (CIMS) was a big step forward for the chemical characterisation of SOA particles as it provides more detailed information about the molecular composition and at the same time records the thermal desorption behaviour (thermogram) of each detected ion. Hence, in addition to composition information, FIGAERO measurements enable the determination of the volatility of SOA constituents as in an ideal case the peak desorption temperature (T_{max}, temperature at peak of ion thermogram) of a single ion thermogram is correlated to the ion volatility expressed by its effective saturation vapour pressure, C_{sat}^* (Lopez-Hilfiker et al., 2014; Schobesberger et al., 2018). This relationship can be calibrated for a specific FIGAERO-CIMS setup and temperature ramp by measuring compounds with known volatilities, e.g. carboxylic acids (Lopez-Hilfiker et al., 2014) or polyethylene glycol (Bannan et al., 2019). Unfortunately, in most cases the data interpretation is more complicated as some compounds will not desorb from the FIGAERO filter at a temperature corresponding to their volatility, but rather decompose at a lower temperature and the decomposition products will be detected in a mass spectrometer (D'Ambro et al., 2019; Lopez-Hilfiker et al., 2015; Stark et al., 2017; Wang and Hildebrandt Ruiz, 2018). The decomposition products may have the exact same sum formula as other constituents of the particles. Thus, only the shape of the ion thermogram may give a hint if an ion stems from desorption (typically sharp peak) or decomposition of one or several different larger compounds (typically broad peak or broad tailing on peak, Schobesberger et al., 2018). Further complication for the interpretation of the T_{max} values arises from the presence of multiple isomers with different volatilities. Depending on how close the T_{max} values of the isomers are and the contribution of each isomer to the signal at this ion mass, the resulting ion thermogram may be multimodal, broadened or with considerable tailing/fronting.

To overcome the issues related to thermal decomposition, and further the interpretation of the ion thermograms, we utilised positive matrix factorization (PMF) in FIGAERO data interpretation. Traditionally, PMF has been used to analyse complex mass spectra datasets mostly to identify the contribution of different sources to the total organic aerosol mass (Jimenez et al., 2009; Lanz et al., 2007; Ulbrich et al., 2009). But for PMF it does not matter if the "source" of a mass spectra signal is a real physical source (e.g. biomass burning, or traffic emissions) or if the source is particles collected on a filter being desorbed. PMF identifies the characteristic changes in the contribution of a source to the total signal, i.e. in the case of FIGAERO-CIMS data one or more compounds desorbing at a specific temperature range. In this study we

apply PMF for the first time in FIGAERO-CIMS data analysis to distinguish the direct desorption (controlled by C_{sat}^*) from the thermal decomposition of thermally labile compounds of lower volatility (controlled by the strength of the weakest bond in the molecule). Further, we combine the FIGAERO-CIMS PMF analysis with the information gained from isothermal evaporation experiments where the particle composition evolves during the isothermal evaporation of the particles to understand processes controlling particle volatility.

2   Methodology

2.1   Dataset

The acquisition of the dataset investigated in this study was described in detail in Buchholz et al. (2019) and in the SI material. The schematic overview of the setup is shown in Figure 1. Briefly, three types of SOA were formed via combined ozonolysis and photooxidation of α-pinene in an oxidative flow reactor (OFR). They are characterised as low-, medium-, and highOC, based on their elemental composition (O:C ratio of 0.53, 0.69, and 0.96, respectively, derived from aerosol mass spectrometer data). A Nano differential mobility analyser (NanoDMA) was used to select a quasi-monodisperse particle distribution (electrical mobility diameter 80 nm) and at the same time dilute the surrounding gas phase by orders of magnitude, which initiates isothermal evaporation at the NanoDMA outlet. The monodisperse particles were then filled into a stainless-steel residence time chamber (RTC) to study their isothermal evaporation behaviour by measuring the particle size in 1 h intervals for up to 10 h. Two sets of evaporation experiments were conducted for each SOA type: dry (RH <2%) and wet (RH80%). To achieve the different RH conditions, only the RH of the sheath flow in the NanoDMA was adjusted, which controls the RH of the selected sample and in the RTC. The conditions of α-pinene SOA formation in the ~~oxidative flow reactor~~ OFR were not changed. Between experiments the instruments, tubing, RTC, and OFR were flushed with particle-free, purified air or nitrogen.

The chemical composition of the particles was investigated directly after the size selection ("fresh" particles, $t_{evap} = 0.25$ h) and after 3 – 4 h of isothermal evaporation in the RTC ("RTC" particles, $t_{evap} = 4$ h) with a filter inlet for gases and aerosols (FIGAERO, Aerodyne Research Inc., Lopez-Hilfiker et al., 2014) sampling unit in combination with a chemical ionisation mass spectrometer (CIMS, Aerodyne Research Inc., Lee et al., 2014) using iodide as reagent ion. Note that the evaporation time of 0.25 h for the "fresh" sample does not stem from residence in the RTC but rather from the collection time on the filter (see SI section 1.1 for details). Due to this minimum evaporation time the FIGAERO-CIMS measurements will underestimate the contribution of volatile compounds in the particles as they leave the OFR.

The combined analysis of evaporation behaviour and FIGAERO-CIMS thermogram and composition information in Buchholz et al. (2019) revealed increasing average desorption temperatures with increasing O:C ratio of the particles while the overall particle volatility (measured by isothermal evaporation) decreased. The residual particles after

4

isothermal evaporation in the RTC exhibited an increase in desorption temperature in all cases indicating that the more volatile species had left the particles. Under wet conditions, evaporation was enhanced due to lowering of particle viscosity and thus kinetic transport limitations as described before (D'Ambro et al., 2018; Wilson et al., 2015; Yli-Juuti et al., 2017). But in the highOC case, strong indications for aqueous phase chemistry were found in the data, namely the shift of some ion thermograms to much higher desorption temperatures and a relative increase in low molecular weight (M_w) compounds. This dataset is thus perfect to test the performance of PMF with FIGAERO-CIMS data: Can PMF capture the evaporation behaviour and separate it from aqueous phase processes in the highOC case?

2.2   FIGAERO-CIMS measurements

It is necessary to understand the operation and data structure of FIGAERO-CIMS to comprehend the challenges of analysing this data with PMF. In the FIGAERO inlet, particles are collected on a PTFE filter. A gradually heated nitrogen gas flow evaporates increasingly less volatile compounds and transports them into the CIMS for detection. In the following, the resulting signal vs desorption temperature curves will be called ion thermogram for individual ions and total thermogram for the sum of all detected ions apart from the reagent ions. Each desorption cycle ("thermogram scan") consists of three parts: the particle collection, the linear increase of the desorption temperature (here, ~25 °C → ~190 °C in 15 min), and a "soak" period at the highest temperature (> 190 °C, 15 min). The soak period ensures that low volatility compounds have been removed from the FIGAERO filter before the next sample is collected. Note that only the part of the thermogram with a near linear increase in the desorption temperature can be used to derive volatility information. The relationship between a compound's desorption temperature, specifically T_{max}, and volatility (e.g. expressed as saturation vapour pressure) can be calibrated for a specific FIGAERO-CIMS setup and temperature ramp, e.g., by measuring polyethylene glycol aerosol with a range of molecular weights and volatilities (similar to the method described by Bannan et al. (2019)).

The raw FIGAERO-CIMS data was processed using tofTools, a MATLAB-based software package developed for analysing ToF-CIMS data (Junninen et al., 2010). The data was averaged to a 20 s time grid, and baseline correction was applied before the high-resolution mass spectra data was fitted. The filter blank measurements were processed in the same fashion as the collected samples. For the PMF analysis, we did not subtract the filter blank measurements but rather added the corresponding filter blank thermograms to the dataset to help with the identification the background factors, i.e., factors dominated by compounds from the instrument and/or filter background (more details on factor identification in section 3.1).

Due to sub-optimal settings in the instrument ion guidance unit, an atypically high amount of declustered ions (not containing the reagent ion iodide) was observed. This was discussed in detail in Buchholz et al. (2019). For this study,

we will not make any assumptions about the declustering process and treat the iodide clusters and declustered ions as separate variables. However, this does not impact the application of PMF to the dataset and the validity of this method for other datasets, as the variables (ions) are all treated independently in the model and variables with the same behaviour will be grouped into the same factor.

2.3   Positive matrix factorisation (PMF)

2.3.1   Working principles of PMF

Since its introduction by Paatero and Tapper (1994), PMF has been established as a useful tool to analyse long time series of mass spectra data mostly from ambient observations.

In the PMF model, it is assumed that the measured data can be expressed by the combination of an (unknown) number p of constant source profiles with varying concentrations over time (Ulbrich et al., 2009). This can be mathematically expressed as:

$$X = GF + E \qquad\qquad (1)$$

X is a $m \times n$ matrix containing the measured mass spectra containing m rows of mass spectra ("observations") each averaged over 20 s of measurement time in the CIMS and n columns representing the time series of one specific ion. G is a $m \times p$ matrix containing the factor time series as columns. The rows of the $p \times n$ matrix F contain the factor mass spectra. Then the $m \times n$ matrix E contains the residuals between the measured data and the fitted values. No a priori information about the values of G and F or the number of factors (p) is required, but the user has to decide which solution (i.e., how many factors) characterises the data best. To account for uncertainties in the measurement data, the PMF model weights the data points with their measurement error (S_{ij}). Values for G and F are constrained to be positive and iteratively found by minimising the quantity, Q, with a least square algorithm (Paatero and Tapper, 1994):

$$Q = \sum_{j=1}^{m} \sum_{i=1}^{n} \left(\frac{E_{ij}}{S_{ij}} \right)^2 \qquad\qquad (2)$$

S_{ij} is the error (uncertainty) of each measurement data point. In an ideal case, the Q value of the model should approach the expected Q value (Q_{exp}) which is equal to the degree of freedom of the model solution. For mass spectra data, this is approximately equal to the size of the original data matrix, X:

$$Q_{exp} \approx n \cdot m \qquad\qquad (3)$$

Different algorithms have been developed to solve the PMF model (e.g. Hoyer, 2004; Lu and Wu, 2004; Paatero, 1999). In this study, we used the PMF2 algorithm with robust, least square optimisation, which is included in the PMF Evaluation Tool (Ulbrich et al., 2009) for Igor Pro 7 (WaveMetrics, Inc., Portland, Oregon). We calculated solutions with 1 to 12

factors. For each solution, 5 rotations (fpeak -1.0 to +1.0) were calculated, and for each original solution (fpeak=0) 6 different seed values were tested.

As an additional measure for the goodness of fit, we calculate the fraction of explained absolute variance ($Ratio_{exp}$):

$$absVar_{total} = \sum_{ij} \left| \boldsymbol{X_{ij}} - \bar{X_\iota} \right| \tag{4}$$

$$absVar_{explained} = \sum_{ij} \left| \boldsymbol{R_{ij}} - \bar{X_\iota} \right| \tag{5}$$

$$Ratio_{exp} = \frac{absVar_{explained}}{absVar_{total}} \tag{6}$$

where $\boldsymbol{R_{ij}}$ is the value in the reconstructed data matrix ($\boldsymbol{R = GF}$) for each ion i and observation j, $\bar{X_\iota}$ is the average measured value of the ion i, $absVar_{total}$ and $absVar_{explained}$ are the total and explained absolute variance. Note that we use the absolute distance between the average values and the measured/reconstructed data instead of the square of this distance.

PMF has been widely used for analysing time series of mass spectra data in the atmospheric science community. However, the model does not utilise the information of the time axis in the optimisation process. Rather, it is a method that can be used to analyse a set of mass spectra which were obtained at different times points during the desorption cycle of FIGAERO and for different particle sampling conditions. This means that PMF will create the same model output if the x values in the data-set are a real time series (Figure 2b), a temperature ramp (Figure 2c) or simply an index with numbers (Figure 2a). Thus, data from separate thermogram scans with FIGAERO-CIMS can be combined to larger datasets and analysed together with PMF. Analysing multiple thermogram scans together has the advantage that more data points are utilised to identify the factors (here, 90 mass spectra for each thermogram) and that factors can be compared directly between scans. Only when evaluating the model output, the real time series/temperature ramp is of interest to interpret the identified factors and compare their desorption temperature profiles between thermogram scans. In the graphic presentation of these combined "time series" (e.g. Figure 4), a data index was used as x values which is the desorption temperature of each thermogram plus an offset (200 per thermogram). This choice of x values preserves the shape of the thermogram in desorption temperature space. The individual thermograms are marked with roman numbers and the sampling conditions are given in the figure captions. For easier comparison of the shape of the desorption behaviour of the factors, they are plotted individually for each SOA type (e.g. Figure 5).

When performing PMF with the combined dataset with all available thermogram scans, the large number of factors (>~~12~~13 or more) necessary to explain the observed variability complicated the analysis and interpretation (see case study in SI section 1.4). Thus, the thermogram scans were grouped by SOA type (i.e., t_{evap} = 0.25 h & 4 h particles, dry & wet conditions of one SOA type: four thermogram scans per group). This pre-grouping reduced the number of factors in each

group enhancing their interpretability while still enabling a direct investigation of the changes due to the evaporation/humidification for one SOA type. But generally, splitting the data by SOA type or even knowing about such different SOA types/sources in the data is not a requirement for analysing a thermogram dataset with PMF.

~~To help with the factor interpretation, the corresponding filter blank measurements were added to these subsets of data.~~
5 ~~Factors with strong contributions to the filter blank scans were considered to be "background" factors, i.e., factors dominated by compounds from the instrument and/or filter background (more details on factor identification in section 3.1).~~

2.3.2 Error schemes for PMF

To perform the PMF analysis, a data error S_{ij} must be defined. As visible from Eq. (2), the S_{ij} values have a strong
10 influence on the outcome of the PMF model. The measurement error can be understood as a weighting mechanism giving more weight to data points with less uncertainty (Paatero and Hopke, 2003). Ideally, S_{ij} is the true measurement error of the dataset. For gas phase CIMS data, Yan et al. (2016) have suggested to calculate the measurement error assuming a Poisson type distribution of the counting error:

$$S_{ij} = a \cdot \sqrt{\frac{X_{ij}}{t_s}} + \sigma_{noise,i} \qquad \textbf{(7)}$$

15 with X_{ij} signal intensity of the ion i, t_s sampling (averaging) interval in s, and $\sigma_{noise,i}$ the electronic noise for ion i. We applied a procedure equivalent to the one introduced by Yan et al. (2016) to derive the parameter a from analysing the distribution of signal noise. The detailed calculation for this type of error is given in the SI material. The resulting error values (Poisson-like, "PLerror") will trace the shape of the thermogram signal with higher absolute values for those parts of the thermogram with higher intensity (i.e., the "peak") giving less weight to this region (Figure S 1). This is the correct
20 approach for the analysis of long time series data where rapid changes are most likely caused by instrument noise or data outliers.

For FIGAERO-CIMS thermograms, the main information lies in the rapidly increasing and decreasing part of the data (the "peak", data points 10 – 50 in Figure 2a) when compounds are desorbing from the FIGAERO filter and not in the slowly changing (or constant) part at high desorption temperatures (the "tail" points 50 – 90 in Figure 2a). During this
25 analysis it was found that the thermal desorption peaks could not be modelled well with error values calculated using Eq 7 (see section 2.3.3 and Appendix A). Thus, a new error scheme that allowed for increased weighting of the thermal desorption peaks was also tested. In this scheme, a constant error value corresponding to the noise in the data at the end of the thermogram scan, is used for each thermogram scan (constant noise, "CNerror") such that:

$$S_{ij} = \sigma_{noise,i} \qquad (8)$$

$\sigma_{noise,i}$ of each ion i is calculated in the same way as for the PLerror (see SI material for details). Note that by omitting the first term in Eq. 7, Eq. 8 does not correspond to the true measurement error of the FIGAERO-CIMS data. Rather, it is the simplest way of weighting the PMF runs to put more emphasis on each thermogram peak and less on the fronts and tails FigureS 1 shows an example of the values for the two error schemes for one exemplary ion. The signal to noise values are up to 3 orders of magnitude higher in the peak region for the CNerror case clearly giving them a stronger weight in the optimisation. As a direct consequence of the modified error value, the value for Q/Q_{exp} is not expected to approach 1, but instead will reach a larger (used error values smaller than real measurement error) or smaller (used error values larger than real measurement error) value. Thus, most solutions from PMF with PLerror will have (much) lower Q and Q/Q_{exp} values than any solution from PMF with CNerror. This also means that comparing the absolute Q or Q/Q_{exp} values between results from the different error schemes is not meaningful as a higher absolute error value will result in a lower Q value.

2.3.3 Selection of error scheme and number of factors ("best" solution)

Before the "best" solution from PMF can be identified by investigating the factor profiles and spectra, the impact of the two different error schemes on the PMF output needs to be determined by running PMF for all combined datasets with both error schemes and comparing the output. As the comparison of the Q/Q_{exp} values between the error schemes is not meaningful, as pointed out above, the fraction of explained variance ($Ratio_{exp}$) and the reconstruction of the characteristic shape of the thermograms (i.e., time series of residuals) were the decisive criteria. In addition to the single Q/Q_{exp} value summed over all ions and observations (i.e., mass spectra) in each dataset, we calculated the time series of the Q contributions (Q_j) summed over all ions for each observation (mass spectrum), j, to identify which periods in the dataset were not captured well by the investigated PMF solution.

$$Q_j = \sum_{i=1}^{n} \left(\frac{E_{ij}}{S_{ij}} \right)^2 \qquad (9)$$

Similarly, we calculate Q_i as the sum over all observations (mass spectra), j, to investigate which ion has the strongest contribution to the overall Q value:

$$Q_i = \sum_{j=1}^{m} \left(\frac{E_{ij}}{S_{ij}} \right)^2 \qquad (10)$$

For a given number of factors, the CNerror scheme results in higher $Ratio_{exp}$ values than the PLerror (Figure 3), i.e., a larger fraction of the observed variance is captured by the model. With the PLerror the maximum $Ratio_{exp}$ is 0.9 even with up to 12 factors while with the CNerror the values for $Ratio_{exp}$ are >0.95 already with 7 factors.

To highlight the difference in behaviour of the two error schemes we display the time series of the residual and Q_j values in Figure 4 for the highOC case for three solutions (6, 7, and 10 factors). With the PLerror, the residuals are much larger than in the CNerror case (panels b and d). But due to the larger values of S_{ij} in the PLerror case, the Q/Q_{exp} values (panels c and e) are much smaller. Thus, the optimisation algorithm sees no need to further improve the model in the PLerror

5   case. Contrarily, the smaller unscaled residual in the 6-factor solution with the CNerror leads to much higher Q/Q_{exp} values, especially in the peak of thermograms III and IV. Here, the addition of one factor (from 6 to 7) improves both the residual and the Q_j/Q_{exp} values, and the new factor captures a characteristic behaviour we discuss below in ~~Section~~ section 3.3.

This analysis together with the more detailed case study in Appendix A leads us to the conclusion that for this study and

10   dataset the CNerror reconstructed the measured data best and yielded the most interpretable results. Thus, from here on we only present results from PMF runs with the CNerror scheme.

The ~~great~~ advantage of PMF, that no a priori information about *F*, *G*, and *p* is needed for the analysis, is also a ~~great~~ disadvantage. There is no absolute criterion for which number of factors (*p*) is correct or "best", but the chosen value ~~greatly~~ strongly impacts the interpretation of the factors and their profiles. In the ideal case, when the true measurement

15   errors are used, Q/Q_{exp} approaches 1 and a solution with Q/Q_{exp} close enough to 1 may be considered as the "best" or correct. But as we explained in the previous paragraph, PMF performed much better for FIGAERO-CIMS data if the "unrealistic" CNerror scheme was used, and thus Q/Q_{exp} are not necessarily meaningful. However, the shape of the Q/Q_{exp} vs number of factors curve can be used to judge the impact of introducing another factor, i.e., a large change in Q/Q_{exp} suggests the new factor explains a large fraction of the variability in the data (Ulbrich et al., 2009). We investigated this

20   for the PMF runs for each SOA type (Figure 3 and Figure S 2). The largest changes in Q/Q_{exp} are achieved already by increasing from 2 to 3 factors. Further factor addition leads to a steady decrease of Q/Q_{exp}. In this case, the $Ratio_{exp}$ values are more helpful. Strong increases of $Ratio_{exp}$ are observed for increasing the number of factors to 6 (medium- and highOC case) or 8 (lowOC case).

As shown by Yan et al. (2016) for gas phase CIMS data, a solution with a low overall Q/Q_{exp} value may still have large

25   variations in the scaled residual with time or with different ions. We carefully investigated especially the time series (Q_j/Q_{exp}) of individual ions (e.g. $C_5H_5O_6^-$ in Figure A 1b and c) and present details of this case study in Appendix A. For each SOA type, there were a few specific ions which were not captured well in the dataset until a certain number of factors was chosen (e.g. 7 in the highOC case) even if the overall fraction of explained variance for the solutions was already larger than 95% and changed very little with further factor addition. We decided to choose the PMF solution with the

30   smallest number of factors which still described the characteristic behaviour of most ion thermograms. These were the solutions with 9, 7, and 7 factors for the low-, medium-, and highOC cases, respectively.

3   Results and Discussion

3.1   PMF factor interpretation

The three evaporation datasets (one for each SOA type) were analysed with PMF using the CNerror scheme and the results for the chosen "best" solutions are shown in Figure 5, Figure 6, and Figure 7 (and with "stacked" factor contribution in Figure S 4, Figure S 5, and Figure S 6). In the following paragraphs, the first letter in the labels of factors indicates if they are from the low- (L), medium- (M) or highOC (H) case, and the second letter identifies the factor type (V, B, D, and C; see below).

Generally, there were three main types of thermogram profiles for all factors: volatility class (type V) with a single, distinct peak (LV1 – 5, MV1 – 5, and HV1 – 5), type background (type B) with mostly constant contribution over the full T_{desorp} range (LB1, MB1, and HB1), and decomposition (type D) with mostly very broad peaks at $T_{desorp} < 65\ °C$ and an increase at $T_{desorp} > 110\ °C$ (LD1, MD1, and HD1).

Factors of type V do not contribute to the filter blank thermograms (Figure S 3) indicating that these factors are linked to compounds only present in the sampled aerosol particles. With the exception of the highOC wet case (which we discuss in detail in ~~Section~~ section 3.3), the peak position (T_{max}) of type V factors changes very little with aerosol age or water content (Table 2). Only the contribution of these factors to the total signal changes with isothermal evaporation or humidification. For each V-type factor, we could identify ions with thermogram shapes similar to the thermogram profile of the individual factors. This means that especially the V-type factors at high desorption temperature are not simply a better mathematical description of the tails of some ion thermograms, but represent real compounds desorbing from the FIGAERO filter at high desorption temperatures. Thus, we interpret the type V factors as volatility classes. Compounds with the same thermal desorption behaviour (i.e., volatility) are grouped into one type V factor which is characterised by its T_{max} value. Note that for the three different SOA types the starting particle composition was significantly different. So even if the T_{max} values for two factors of different SOA type, e.g., LV2, MV2, and HV1(dry cases), differ only by ~5 °C, the compounds contributing to them are not the same, i.e., the factor mass spectra for LV2, MV2, and HV1 are significantly different. We elaborate on the reasons for these differences in SI section 1.3 and 1.4.

Type B factors show contributions to the signal of sample thermograms and filter blanks (Figure S 3). For LB1, MB1, and HB1, the very shallow thermogram profile and the similar absolute signal strength despite different mass loadings on the FIGAERO filter indicate that these are instrument background factors. For all SOA types, the mass spectra of these factors are dominated by single ions typically associated with FIGAERO-CIMS background (e.g. fluorine containing compounds, formic acid, and lactic acid). According to the uncentered correlation method (contrast angle/ dot product) MB1 and HB1 are reasonably similar. For the lowOC case, some of the instrument background is apparently assigned to

11

the contamination factors (LC1&2, see below), thus decreasing the degree of similarity between LB1 and the other B factors.

Type D factors are the most difficult to interpret as they have contribution to the signal for both filter blank and sample thermograms, but the contribution can vary with the collected mass loading on the filter for sample thermograms. The

5 factor mass spectra (LD1, MD1, and HD1) show mostly contribution from ions with $M_w < 200$ Da, but the thermogram profiles exhibit a strong increase at $T_{desorp} > 110$ °C especially in filter blank thermograms. This suggests that the detected low M_w compounds in these factors are thermal decomposition products of larger, low volatile, but thermally unstable compounds. But in some cases (e.g. mediumOC dry, $t_{evap} = 0.25$ h and 4 h, Figure 6a and b) there is a second peak at much lower T_{desorp} (< 65 °C) which is in the range where compounds of the detected composition are expected to desorb.

10 This suggests that the ions grouped into the type D factors can stem from two "sources" – direct desorption ($T_{desorp} < \sim100$ °C) and thermal decomposition ($T_{desorp} > \sim100$ °C) – and PMF is not able to separate them as either their composition or their desorption behaviour is too similar. Consequently, type D factors have to be analysed carefully and interpreted as desorption at low T_{desorp} and decomposition at high T_{desorp}. Also, the instrument background contribution needs to be estimated from the filter blank thermograms. For the lowOC case, LD1 is dominated by compounds coming

15 from the filter/instrument background as the factor thermogram profile does not change with the collected sample mass and there is still contribution of the factor below $T_{desorp} < 100$ °C after 4 h of isothermal evaporation (Figure S 3a). For mediumOC, the direct desorption part ($T_{desorp} < 100$ °C) of MD1 is removed with isothermal evaporation which suggests that at least this part of the factor stems from the collected sample and not just the instrument/filter background. The highOC case is discussed below in section 3.3.

20 For the lowOC dry, $t_{evap} = 0.25$ h sample, two additional factors (type C) were found. The factor mass spectra of LC1&2 are dominated by extremely high signals for formic and lactic acid, which are typically strong indications of a contamination on the FIGAERO filter due to handling. We could not determine in retrospect what happened to this specific sample collection to cause this obvious contamination, but between this and the next sample collection the FIGAERO filter was replaced, and several heating cycles were performed ensuring that no other sample was affected.

25 However, since PMF has identified the ions affected by this contamination and grouped them into LC1&2, these two factors can be omitted from further analysis removing the bias caused by this contamination.

Note that almost the same factors are produced by PMF independent of whether the filter blank measurements are added to the datasets or not. This shows that PMF can be a very helpful tool for data interpretation when no reliable instrument background measurements are available, or if the background varies strongly between samples. Then the identification of

30 B, D, and C type factors has to rely only on the thermogram profiles and factor mass spectra.

3.2   Composition changes due to evaporation

One set of type V factors (i.e., volatility classes) was identified and separated from instrument background contributions for each dataset consisting of one SOA type sampled after different time intervals of isothermal evaporation under dry and wet conditions. The contribution of a single factor to the total signal is calculated as the ratio of the integral of the thermogram profile of this factor to the total signal. The relative contribution of factors V1 – V5 for each sampling condition is shown in Figure 8 plotted vs the volume fraction remaining (VFR) measured in separate isothermal evaporation measurements (VFR values from Buchholz et al. (2019)). The corresponding figure with absolute signal contributions is shown in the SI material (Figure S 7). Note that always the residual particles after isothermal evaporation or humidification were collected on the FIGAERO filter. This means with decreasing VFR a larger fraction of the particle mass had evaporated prior to the FIGAERO-CIMS measurements. In the low- and mediumOC case (Figure 8a and b), the relative contributions of MV1&2 and LV1&2 (T_{max} in SVOC range) decreased with decreasing VFR while those of LV3-5 and MV3-5 (T_{max} in LVOC and ELVOC range) increased. During 4 h of dry isothermal evaporation a similar volume fraction was removed as in 0.25 h of isothermal evaporation under wet conditions. The very similar relative contribution of the V-type factors in these two samples suggests that the observed changes in chemical composition in the particles are indeed connected to the change in VFR (i.e., how much of the volatile material was removed before sampling) and not directly driven by other water induced processes. For these SOA types, the main process during physical aging in the RTC (i.e., long residence time in clean air) under dry and wet conditions was isothermal particle evaporation. Here, the particulate water mostly decreased the viscosity in the particles, thus decreasing kinetic transport limitations in the particle phase and increasing evaporation. This observation is in agreement with previous interpretation of this and comparable datasets (Buchholz et al., 2019; Yli-Juuti et al., 2017). The highOC case (Figure 8c) will be discussed in ~~Section~~ section 3.3.

From the factor contribution, the detailed changes in particle composition due to isothermal evaporation can be derived by analysing the trends in the factor mass spectra. With increasing T_{max} of the factors (i.e., decreasing volatility) the average M_w as well as the C chain length and number of O continuously increased from V1 to V5 (Table 1). The contribution of compounds with C>10 also increased, which suggests an increasing contribution of dimers/oligomers. This may explain why no clear trend in the O:C (or OS_c) values could be observed for the V-type factors. While the lower volatility compounds indeed contained more oxygen the simultaneous increase of the carbon chain length seems to compensate this, resulting in no obvious systematic increase in O:C ratios. Thus, we observe a correlation of volatility with average M_w but not with average O:C ratio of the factors.

As the more volatile factors (LV1&2 and MV1&2) were systematically removed with isothermal evaporation, the composition of the residual particles was more and more dominated by the less volatile factors (LV3-5 and MV3-5), i.e.,

by larger, higher M_w compounds, many of them dimers/oligomers. However, the V4&5 factors still had a significant contribution of low M_w compounds as well (Figure 5 and Figure 6). The ion and factor thermograms of $[C_8H_{12}O_5 + I]^-$ are shown as an example for such a relatively small, low M_w ion in Figure 9a and b. This ion had contributions to all 5 factors. In principle, it is possible that there are several isomers of this composition with significantly different volatility being grouped into V1-5 spreading ~4 orders of magnitude in C^*. But it seems more likely that the compounds of this composition contributing to V4&5 were products of thermal decomposition. If this was indeed the case, it means that there were compounds in the particles which have a volatility corresponding to even higher T_{max} than that of factors V4&5, but because they decompose at desorption temperatures >100 °C they are grouped into these factors/volatility classes. This is an indication that FIGAERO-CIMS data overestimates the volatility as already previously suggested (Lopez-Hilfiker et al., 2015; Schobesberger et al., 2018; Stark et al., 2017), and care has to be taken when using these volatility values for modelling purposes.

3.3   Composition changes due to aqueous phase chemistry

Similar to the low- and mediumOC case, highOC SOA particles showed enhanced evaporation under wet conditions (Buchholz et al., 2019). But in addition, strong signs for aqueous phase chemistry in the wet highOC case were already visible by comparing the mass spectra integrated over the whole thermogram scan. Several very small compounds ($M_w <$ 200 Da and C_4-C_7) increased their contribution under wet conditions. Also, the thermograms of these ions showed distinct shifts to higher T_{max} values in the wet cases (by up to 20 °C) and even the formation of new low volatility material under wet conditions. As discussed by Buchholz et al. (2019), the different behaviour of the highOC SOA is most likely due to higher fractions of (hydro-)peroxides in the particles caused by the much higher HO_2 concentrations in the OFR at the highOC oxidation conditions. Most peroxides are sensitive to hydrolysis which will initiate a range of reactions in the aqueous phase. The low volatility products of these reactions thermally decompose to similar fragments as did the peroxide precursor. Thus, the same groups of ions are detected but at a higher T_{desorp}.

In the PMF analysis results, ~~this~~ the different behaviour in the highOC case is also directly visible comparing the dry, $t_{evap} = 0.25$ h and wet, $t_{evap} = 0.25$ h cases (Figure 7a and c). The contribution of the (semi-)volatile factor (HV1) is reduced, but the factor thermogram profile and T_{max} also change. HV2&4 shift to higher T_{max} values and a new factor HV3 is introduced which contains mostly low M_w compounds. The least volatile factor, HV5, which contains mostly high M_w compounds, shows much less contribution. It is also noteworthy that HD1 shows a strong increase in the wet case, not just in relative contribution but also in absolute strength. Also, the shape of the factor thermogram profile (strong increase at $T_{desorp} > 100$ °C) indicates that in this case HD1 is dominated by thermal decomposition products. With further

isothermal evaporation under wet conditions, HV3 increased its contribution while HV1&2 were almost completely removed (Figure 7 and Figure 8). Note that HV3 also exhibits an increase in absolute contribution to the signal, i.e., compounds contributing to this factor are being produced (Figure S 7c).

The removal of HV1 can still be explained by particulate water acting as a plasticiser enhancing the isothermal evaporation comparable to the low- and mediumOC cases. But HV2 has a T_{max} value already in the LVOC range like LV3 or MV3, which do not show a similar decrease with isothermal evaporation under wet conditions. Thus, the observed changes can only be explained by chemical processes induced by the presence of water in the particles. These processes consume compounds which were mostly grouped into factors HV2 and HV5. The T_{max} shift of HV1 and HV4 indicates that some compounds grouped into these factors might have been affected as well. The reaction products are mostly detected as low M_W compounds in HV3 and HD1. While the compounds grouped into HV3 might still be desorbing as such from the filter, this seems extremely unlikely for the compounds in HD1 as it only starts to appear at desorption temperatures > 100 °C. Thus, many of the formed low volatility compounds must be thermally unstable.

In our previous work (Buchholz et al., 2019), we used the unexpectedly large shift of T_{max} of specific ions together with the formation of low volatile material at wet conditions as evidence for aqueous phase chemistry in the highOC case. With the results from PMF we can now show how this T_{max} shift in the highOC case is indeed different from those smaller ones observed for the other SOA types. The single ion thermograms for $[C_8H_{12\theta}O_5+I]^-$ (strong ion in low- and mediumOC samples) and for $C_4H_3O_6^-$ (strong ion in highOC identified to be affected by aqueous chemistry) are shown in Figure 9. In the low- and mediumOC cases (Figure 9a and b), T_{max} changed by ~10 °C between the sample with least (dry, t_{evap} = 0.25 h) and with most isothermal evaporation (wet, t_{evap} = 4 h). This shift is solely caused by the removal of LV1&MV1 and partly LV2&MV2, i.e., by the isothermal evaporation of the volatile fraction at this composition. In the highOC case (Figure 9c), HV1 is also removed with isothermal evaporation, but the new factor HV3 dominates under wet conditions. The change in T_{max} by 40 °C between the dry, t_{evap} = 0.25 h case when HV1 dominates and the wet, t_{evap} = 4 h case when HV3 is the only contribution is then simply the difference in volatility between the original compounds detected with this composition and the ones formed by aqueous phase chemistry.

In the dry case, there is a small contribution of HV3 around 100 °C. This is most likely due to the described aqueous phase processes happening already inside the OFR which was operated at ~40% RH. The drying during size selection stopped these processes leading to very minor contribution of the reaction products to the particle phase. If the particle stayed at wet conditions, the reactions continued and created the compounds grouped into HV3. But apart from this, there has to be another source for the compounds in HV3 in the dry case as there is a small peak at 63 °C. However, this peak is a very minor contribution to the overall signal in the dry case while HV3 at 100 °C dominates the thermograms in the wet case.

4   Conclusions

To our knowledge, this is the first study applying a PMF analysis to high resolution FIGAERO-CIMS thermal desorption data and interpreting the PMF factors as volatility classes characterised by their T_{max} values. Although we used a very specific dataset from a focussed laboratory study, the introduced method can be applied to other FIGAERO-CIMS datasets. The nature of PMF allows to combine multiple separate FIGAERO-CIMS thermograms and investigate them together.

We found that it is very important to study the impact of the chosen "measurement error" on the PMF solutions before interpreting the results of the PMF analysis. Instead of the most realistic measurement error, an error scheme best suited to focus on the part of the data relevant to the research question should be chosen. In our case, the most interpretable results were achieved by applying a CNerror based on the noise of each ion.

PMF was able to separate the measured signal of each ion into instrument background, contamination, and collected aerosol mass. This separation worked even if no filter blank data was added to the datasets. However, adding filter blank measurements to the dataset simplified the identification of background factors. Identifying background factors in this way instead of simply subtracting periodically taken filter blank measurements is especially helpful, if an insufficient number of filter blank measurements were collected or if the background changed between filter blank samples. Being able to determine the actual contribution of background compounds becomes even more important for low concentration measurements (i.e., low collected sample mass on the FIGAERO filter). At low concentrations, the shape of the combined thermogram of the background may significantly alter the overall shape of the thermogram (e.g., shift the T_{max} value) and thus change the interpretation of the volatility of the collected aerosol.

The collected aerosol mass signal part was separated into (mostly) direct desorption factors (i.e., volatility classes) and thermal decomposition factors. Thermal decomposition became the dominant process for many low M_w ions observed at temperatures above 120 °C. Then the observed "desorption" temperatures are actually the decomposition temperatures and thus give an upper limit for the true volatility of the parent compounds. This shows again that FIGAERO-CIMS measurements may overestimate the volatility of aerosol particles based on parameterisation of the overall composition but also on desorption temperatures as described by some previous studies (Lopez-Hilfiker et al., 2016; Schobesberger et al., 2018; Stark et al., 2017). The knowledge about the contribution of thermal decomposition to a thermogram measurement obtained with the PMF method presented here can be used e.g. to improve the input into process models. An example for such an application is presented in (Tikkanen et al., (2019).

For each SOA type (i.e., α-pinene SOA of different oxidative age) 5 main volatility classes were identified in the chosen PMF solution. Isothermal evaporation prior to sampling with FIGAERO-CIMS systematically removed the more volatile factors with T_{max} values corresponding to SVOCs. Low M_w compounds remaining in the particles after evaporation were

16

attributed to low volatility factors indicating that they most likely were products of thermal decomposition above ~100 °C. However, between ~100 and 120 °C thermal decomposition was still a minor process. In the highOC case, the aqueous phase chemistry occurring under wet conditions was captured by introducing a new factor and shifts in T_{max} for other factors. Both the educts and products (or thermal decomposition products of them) could be identified. This highlights how PMF analysis can help with identifying processes in the particle phase.

The highOC SOA in our study may not be representative of ambient SOA of the same OC ratio as it was formed under extremely strong oxidation conditions in an OFR. But the type of compounds affected by aqueous phase chemistry (i.e., organic compounds containing (hydro)peroxides or other functional groups which easily hydrolyse and then continue to react) are not unique to OFR reactors. One formation path of compounds containing several hydroperoxyl or peroxiacid groups is the auto-oxidation of terpenes in the gas-phase leading to highly oxygenated material (HOM) (Bianchi et al., 2019; Ehn et al., 2014). These compounds play an important role in particle growth and detected more and more in ambient measurements (Lee et al., 2018; Mohr et al., 2017). Another compound class which is possibly susceptible to hydrolysis is organo-nitrates (which did not occur in our study due to the experiment design). Thus, ambient aerosol will probably not show as clear signs of aqueous phase chemistry as our high OC case, but it is very likely that such processes occur to some degree and may be detected with the PMF analysis of FIGAERO thermogram data.

We like to point out that picking the "best" solution of PMF may have subjective bias and that there is no guarantee that we selected the truly optimal solution. But even if a higher number of factors was chosen, the overall interpretation of the factors was the same as the additional factors were added in all thermograms in the dataset typically splitting one of the previously identified factors. The influence of the background and thermal decomposition was still separated from the V-type factor and within one set of V-type factors for one SOA type there was very little variation in T_{max} values. Different degrees of isothermal evaporation of the particles prior to FIGAERO sampling were still reconstructed by decreasing the contribution of the most volatile factors. If chemical processes altered the particle composition enough, one or more separate "wet chemistry" factor(s) were introduced and some of the other factors shift their T_{max}. Thus, even without a hard criterion to determine the "correct" number of factors, the PMF analysis of FIGAERO-CIMS data gives valuable insights into processes in the particle phase.

The example ions shown in Figure 9 highlight how important it is to allow a single ion to contribute to more than one class/factor when analysing FIGAERO-CIMS data. Clustering techniques, as for example described by Koss et al. (2019) or Li et al. (2019), which assign each detected ion/composition to a single cluster, are incapable of capturing such a behaviour, i.e., the shift of T_{max} between two measured thermograms due to the selective removal of some of the isomers/thermal decomposition products. For the investigated dataset, we artificially removed the volatile fraction at a

17

set ion composition with the prior isothermal evaporation. However, as the composition of ambient aerosol changes with time, e.g. by changes in the gas-particle partitioning or due to aging processes, the ratio between different isomers or the educts for thermal decomposition will change causing similar features in single ion thermograms of FIGAERO-CIMS data. A careful PMF analysis of the thermogram data will reveal the changes in volatility and the contribution of thermal decomposition to the signal in addition to information about changes in the physical sources of the organic material. Preliminary tests with a dataset of ambient FIGAERO-CIMS measurements show how PMF immediately separates the data by its ambient sources (i.e., which precursors and/or processes created the aerosol) and/or SOA type (e.g. fresh and aged OA). This information is also accessible with a PMF analysis of the time series of mass spectra integrated for each desorption cycle. However, in addition to this, PMF of the thermal desorption data provides detailed information on the volatility of each of these sources or SOA types while also showing how much of the signal is affected by thermal decomposition. This information on the contribution of thermal decomposition is crucial when the FIGAERO-CIMS data is used to identify the detailed composition or volatility of SOA particles. Details of this investigation will be the content of a future publication.

Appendix A Case study on impact of different error schemes

As briefly described in sections 2.3.2 and 2.3.3, we investigated the impact of two different error schemes (CNerror and PLerror) on the results of PMF. The highOC dataset was selected for this case study as the ions affected by aqueous phase chemistry proved to be the most difficult to capture.

In the PLerror case, the residual time series for the total ion signal (Figure 4d) was positive at all times (i.e., the total reconstructed signal was lower than the measured data) and decreased very little when increasing the factor number from 6 to 10. While the residual time series of individual ions did exhibit negative values (Figure A 1d and Figure A 2d), their distribution was still biased towards positive values (i.e., overall under-predicting the measured data). In the CNerror case (Figure 4b), in particular, the residual time series is spread more symmetric around 0 and additionally exhibits much lower values than in the comparable PLerror case, particularly for thermograms III and IV (particles under wet conditions).

To illustrate why there is no further improvement in the PMF results with the PLerror scheme and to show at which part of the dataset the error schemes create different results, we investigate the behaviour of the PMF solutions for individual ions. We select two ions with similar signal strength. One characteristic for ions captured well with both error schemes ($[C_7H_8O_6 + I]^-$, Figure A 2) and one ($C_5H_5O_6^-$, Figure A 1) where the PLerror scheme does not perform well. Note that the later represents the group contained mostly ions which were affected by aqueous phase chemistry. For the 6-factor solution (red line in Figure A 1b and d), the residual time series for this ion have similar values for thermogram scans III and IV in both error schemes, but increasing the numbers of factors by 1 seems to have a noticeable effect only in the

18

CNerror case. This is because here, the Q_{ion} values ($Q_{ion} = \left(\frac{E_{ion}}{S_{ion}}\right)^2$) are extremely high for that part of the dataset (red line panel c). Investigating the Q_i values summed over all observations (mass spectra) show that this ion ($C_5H_5O_6^-$) has the 5th highest contribution to overall Q/Q_{exp}. The other ions with such high single contribution to Q/Q_{exp} exhibit very similar behaviour of their residuals and Q_{ion} values. Together they account for 15% of the overall Q/Q_{exp} value in the 6-factor case. So, adding an additional factor describing that portion of the dataset will strongly decrease Q_{ion} and with it Q/Q_{exp} indicating a better fit. In the PLerror case, the Q_{ion} values exhibit very similar profiles for all four thermogram scans (Figure A1d and e). Thus, changing any parameter for $C_5H_5O_6^-$ will have little effect on the Q_{ion} values and therefore on overall Q/Q_{exp}. This example clearly shows how the selection of the error values guides the focus of PMF, i.e., which part of the dataset still needs improvement when the number of factors is increased. In Figure A 3, the contribution of each factor to the signal of $C_5H_5O_6^-$ is shown by coloured areas for the 6 (top) and 7 (bottom) factor solutions for CNerror (a and c) and PLerror (b and d) to highlight the change between 6 and 7 factors for this ion. In addition to reducing the residual for the peaks in thermograms III and IV, using CNerror, the additional factor substantially alters the factor time series for this ion, therefore likely affecting our interpretation of these factors, presumably towards improved accuracy. Indeed the "new" factor F3 was identified in section 3.3 as HV3 containing the products of the chemical reactions in the aqueous phase.

This error scheme depending performance of PMF is not controlled by the signal strength of the ion or the ratio between signals of combined thermograms. The two example ions were chosen explicitly because of their similar signal strength in all thermograms (compare Figure A 1a and Figure A 2a). It rather seems that the PLerror does not assign enough weight to the peak region of the ion thermograms. Thus, it cannot resolve the changes in peak shape (i.e., the large shift towards higher desorption temperatures). As the shift is caused by specific processes in the particle phase, PMF with the PLerror will not identify these processes.

These two observations, the CNerror explaining more of the observed variance in general and capturing the complex chemical processes in the particles, leads us to the conclusion that for this study and dataset the CNerror yields the more interpretable results and should be used. Even though it is not be the "true" measurement error of the data.

Appendix B Mathematical symbols

Table B1 Mathematical symbols and notations used in the equations throughout the paper.

symbol	explanation
X, X_{ij}	data matrix (*n x m*) and data matrix element
p	number of factors
m	number of observations (mass spectra) in the dataset
n	number of ions in the dataset
G	factorization matrix containing the factor thermograms as columns (*n x p*)
F	factorization matrix containing the factor mass spectra as rows (*p x m*)
E, E_{ij}	residual matrix and residual matrix element
R, R_{ij}	reconstructed data matrix ($R = GF$) and reconstructed data matrix element
S, S_{ij}	measurement error matrix and error matrix element
$absVar_{total}$	total absolute variance
$absVar_{exp}$	explained absolute variance
$Ratio_{exp}$	Ratio of explained to total absolute variance
Q	square of the residual scaled with the error summed over all ions and observations (mass spectra)
Q_{exp}	expected Q value, in the ideal case with the "true" measurement error equal to *n x m*
Q_j	square of the residual scaled with the error summed over all observations (mass spectra)
Q_i	square of the residual scaled with the error summed over all ions
Q_{ion}	square of the residual scaled with the error for a single ion as time series
Q/Q_{exp}	optimisation parameter in PMF

5

5   References

Bannan, T. J., Le Breton, M., Priestley, M., Worrall, S. D., Bacak, A., Marsden, N. A., Mehra, A., Hammes, J., Hallquist, M., Alfarra, M. R., Krieger, U. K., Reid, J. P., Jayne, J., Robinson, W., McFiggans, G., Coe, H., Percival, C. J. and Topping, D.: A method for extracting calibrated volatility information from the FIGAERO-HR-ToF-CIMS and its
10   experimental application, Atmos. Meas. Tech., 12(3), 1429–1439, doi:10.5194/amt-12-1429-2019, 2019.

Bianchi, F., Kurtén, T., Riva, M., Mohr, C., Rissanen, M. P., Roldin, P., Berndt, T., Crounse, J. D., Wennberg, P. O., Mentel, T. F., Wildt, J., Junninen, H., Jokinen, T., Kulmala, M., Worsnop, D. R., Thornton, J. A., Donahue, N., Kjaergaard, H. G. and Ehn, M.: Highly Oxygenated Organic Molecules (HOM) from Gas-Phase Autoxidation Involving Peroxy Radicals: A Key Contributor to Atmospheric Aerosol, Chem. Rev., 119(6), 3472–3509,
15   doi:10.1021/acs.chemrev.8b00395, 2019.

Buchholz, A., Lambe, A. T., Ylisirniö, A., Li, Z., Tikkanen, O. P., Faiola, C., Kari, E., Hao, L., Luoma, O., Huang, W., Mohr, C., Worsnop, D. R., Nizkorodov, S. A., Yli-Juuti, T., Schobesberger, S. and Virtanen, A.: Insights into the O: C-dependent mechanisms controlling the evaporation of α-pinene secondary organic aerosol particles, Atmos. Chem. Phys., 19(6), 4061–4073, doi:10.5194/acp-19-4061-2019, 2019.

20   D'Ambro, E. L., Schobesberger, S., Zaveri, R. A., Shilling, J. E., Lee, B. H., Lopez-Hilfiker, F. D., Mohr, C. and Thornton, J. A.: Isothermal Evaporation of α-Pinene Ozonolysis SOA: Volatility, Phase State, and Oligomeric Composition, ACS Earth Sp. Chem., 2(10), 1058–1067, doi:10.1021/acsearthspacechem.8b00084, 2018.

D'Ambro, E. L., Schobesberger, S., Gaston, C. J., Lopez-Hilfiker, F. D., Lee, B. H., Liu, J., Zelenyuk, A., Bell, D., Cappa, C. D., Helgestad, T., Li, Z., Guenther, A., Wang, J., Wise, M., Caylor, R., Surratt, J. D., Riedel, T., Hyttinen, N., Salo,
25   V.-T., Hasan, G., Kurtén, T., Shilling, J. E. and Thornton, J. A.: Chamber-based insights into the factors controlling IEPOX SOA yield, composition, and volatility, Atmos. Chem. Phys. Discuss., (August), 1–20, doi:10.5194/acp-2019-271, 2019.

Donahue, N. M., Robinson, A. L., Stanier, C. O. and Pandis, S. N.: Coupled partitioning, dilution, and chemical aging of semivolatile organics, Environ. Sci. Technol., 40(8), 2635–2643, doi:10.1021/es052297c, 2006.

30   Ehn, M., Thornton, J. A., Kleist, E., Sipilä, M., Junninen, H., Pullinen, I., Springer, M., Rubach, F., Tillmann, R., Lee, B., Lopez-Hilfiker, F., Andres, S., Acir, I. H., Rissanen, M., Jokinen, T., Schobesberger, S., Kangasluoma, J., Kontkanen, J., Nieminen, T., Kurtén, T., Nielsen, L. B., Jørgensen, S., Kjaergaard, H. G., Canagaratna, M., Maso, M. D., Berndt, T., Petäjä, T., Wahner, A., Kerminen, V. M., Kulmala, M., Worsnop, D. R., Wildt, J. and Mentel, T. F.: A large source of low-volatility secondary organic aerosol, Nature, 506(7489), 476–479, doi:10.1038/nature13032, 2014.

35   Glasius, M. and Goldstein, A. H.: Recent Discoveries and Future Challenges in Atmospheric Organic Chemistry, Environ. Sci. Technol., 50(6), 2754–2764, doi:10.1021/acs.est.5b05105, 2016.

Goldstein, A. H. and Galbally, I. E.: Known and Unexplored Organic Constituents in the Earth's Atmosphere, Environ. Sci. Technol., 41(5), 1514–1521, doi:10.1021/es072476p, 2007.

Herrmann, H.: Kinetics of Aqueous Phase Reactions Relevant for Atmospheric Chemistry, Chem. Rev., 103(12), 4691–4716, doi:10.1021/cr020658q, 2003.

Hoyer, P. O.: Non-negative matrix factorization with sparseness constraints, J. Mach. Learn. Res., 5, 1457–1469, 2004.

Jimenez, J. L., Canagaratna, M. R., Donahue, N. M., Prevot, A. S. H., Zhang, Q., Kroll, J. H., DeCarlo, P. F., Allan, J. D., Coe, H., Ng, N. L., Aiken, A. C., Docherty, K. S., Ulbrich, I. M., Grieshop, A. P., Robinson, A. L., Duplissy, J., Smith, J. D., Wilson, K. R., Lanz, V. A., Hueglin, C., Sun, Y. L., Tian, J., Laaksonen, A., Raatikainen, T., Rautiainen, J., Vaattovaara, P., Ehn, M., Kulmala, M., Tomlinson, J. M., Collins, D. R., Cubison, M. J., Dunlea, J., Huffman, J. A., Onasch, T. B., Alfarra, M. R., Williams, P. I., Bower, K., Kondo, Y., Schneider, J., Drewnick, F., Borrmann, S., Weimer, S., Demerjian, K., Salcedo, D., Cottrell, L., Griffin, R., Takami, A., Miyoshi, T., Hatakeyama, S., Shimono, A., Sun, J. Y., Zhang, Y. M., Dzepina, K., Kimmel, J. R., Sueper, D., Jayne, J. T., Herndon, S. C., Trimborn, A. M., Williams, L. R., Wood, E. C., Middlebrook, A. M., Kolb, C. E., Baltensperger, U. and Worsnop, D. R.: Evolution of Organic Aerosols in the Atmosphere, Science (80-.)., 326(5959), 1525–1529, doi:10.1126/science.1180353, 2009.

Junninen, H., Ehn, M., Petäjä, Luosujärvi, L., Kotiaho, T., Kostiainen, R., Rohner, U., Gonin, M., Fuhrer, K., Kulmala, M. and Worsnop, D. R.: A high-resolution mass spectrometer to measure atmospheric ion composition, Atmos. Meas. Tech., 3(4), 1039–1053, doi:10.5194/amt-3-1039-2010, 2010.

Koss, A. R., Canagaratna, M. R., Zaytsev, A., Krechmer, J. E., Breitenlechner, M., Nihill, K., Lim, C., Rowe, J. C., Roscioli, J. R., Keutsch, F. N. and Kroll, J. H.: Dimensionality-reduction techniques for complex mass spectrometric datasets: application to laboratory atmospheric organic oxidation experiments, Atmos. Chem. Phys. Discuss., (June), 1–42, doi:10.5194/acp-2019-469, 2019.

Kroll, J. H. and Seinfeld, J. H.: Chemistry of secondary organic aerosol: Formation and evolution of low-volatility organics in the atmosphere, Atmos. Environ., 42(16), 3593–3624, doi:10.1016/j.atmosenv.2008.01.003, 2008.

Lanz, V. A., Alfarra, M. R., Baltensperger, U., Buchmann, B., Hueglin, C. and Prévôt, A. S. H.: Source apportionment of submicron organic aerosols at an urban site by factor analytical modelling of aerosol mass spectra, Atmos. Chem. Phys., 7(6), 1503–1522, doi:10.5194/acp-7-1503-2007, 2007.

Lee, B. H., Lopez-Hilfiker, F. D., Mohr, C., Kurtén, T., Worsnop, D. R. and Thornton, J. A.: An iodide-adduct high-resolution time-of-flight chemical-ionization mass spectrometer: Application to atmospheric inorganic and organic compounds, Environ. Sci. Technol., 48(11), 6309–6317, doi:10.1021/es500362a, 2014.

Lee, B. H., Lopez-Hilfiker, F. D., D'Ambro, E. L., Zhou, P., Boy, M., Petäjä, T., Hao, L., Virtanen, A. and Thornton, J. A.: Semi-volatile and highly oxygenated gaseous and particulate organic compounds observed above a boreal forest canopy, Atmos. Chem. Phys., 18(15), 11547–11562, doi:10.5194/acp-18-11547-2018, 2018.

Li, Z., D'Ambro, E. L., Schobesberger, S., Gaston, C. J., Lopez-Hilfiker, F. D., Liu, J., Shilling, J. E., Thornton, J. A. and Cappa, C. D.: A robust clustering algorithm for analysis of composition-dependent organic aerosol thermal desorption measurements, Atmos. Chem. Phys. Discuss., (September), 1–52, doi:10.5194/acp-2019-733, 2019.

Liu, P., Li, Y. J., Wang, Y., Gilles, M. K., Zaveri, R. A., Bertram, A. K. and Martin, S. T.: Lability of secondary organic particulate matter, Proc. Natl. Acad. Sci. U. S. A., 113(45), 12643–12648, doi:10.1073/pnas.1603138113, 2016.

Lopez-Hilfiker, F. D., Mohr, C., Ehn, M., Rubach, F., Kleist, E., Wildt, J., Mentel, T. F., Lutz, A., Hallquist, M., Worsnop, D. and Thornton, J. A.: A novel method for online analysis of gas and particle composition: description and evaluation of a Filter Inlet for Gases and AEROsols (FIGAERO), Atmos. Meas. Tech., 7, 983–1001, doi:10.5194/amt-7-983-2014, 2014.

Lopez-Hilfiker, F. D., Mohr, C., Ehn, M., Rubach, F., Kleist, E., Wildt, J., Mentel, T. F., Carrasquillo, A. J., Daumit, K.

E., Hunter, J. F., Kroll, J. H., Worsnop, D. R. and Thornton, J. A.: Phase partitioning and volatility of secondary organic aerosol components formed from α-pinene ozonolysis and OH oxidation: The importance of accretion products and other low volatility compounds, Atmos. Chem. Phys., 15(14), 7765–7776, doi:10.5194/acp-15-7765-2015, 2015.

Lopez-Hilfiker, F. D., Mohr, C., D'Ambro, E. L., Lutz, A., Riedel, T. P., Gaston, C. J., Iyer, S., Zhang, Z., Gold, A., Surratt, J. D., Lee, B. H., Kurten, T., Hu, W. W., Jimenez, J., Hallquist, M. and Thornton, J. A.: Molecular Composition and Volatility of Organic Aerosol in the Southeastern U.S.: Implications for IEPOX Derived SOA, Environ. Sci. Technol., 50(5), 2200–2209, doi:10.1021/acs.est.5b04769, 2016.

Lu, J. and Wu, L.: Technical details and programming guide for a general two-way positive matrix factorization algorithm, J. Chemom., 18(12), 519–525, doi:10.1002/cem.894, 2004.

Mohr, C., Lopez-Hilfiker, F. D., Yli-Juuti, T., Heitto, A., Lutz, A., Hallquist, M., D'Ambro, E. L., Rissanen, M. P., Hao, L., Schobesberger, S., Kulmala, M., Mauldin, R. L., Makkonen, U., Sipilä, M., Petäjä, T. and Thornton, J. A.: Ambient observations of dimers from terpene oxidation in the gas phase: Implications for new particle formation and growth, Geophys. Res. Lett., 44(6), 2958–2966, doi:10.1002/2017GL072718, 2017.

Paatero, P.: The Multilinear Engine—A Table-Driven, Least Squares Program for Solving Multilinear Problems, Including the n-Way Parallel Factor Analysis Model, J. Comput. Graph. Stat., 8(4), 854–888, doi:10.1080/10618600.1999.10474853, 1999.

Paatero, P. and Hopke, P. K.: Discarding or downweighting high-noise variables in factor analytic models, in Analytica Chimica Acta, vol. 490, pp. 277–289, Elsevier., 2003.

Paatero, P. and Tapper, U.: Positive matrix factorization: A non-negative factor model with optimal utilization of error estimates of data values, Environmetrics, 5(2), 111–126, doi:10.1002/env.3170050203, 1994.

Pankow, J. F.: An absorption model of gas/particle partitioning of organic compounds in the atmosphere, Atmos. Environ., 28(2), 185–188, doi:10.1016/1352-2310(94)90093-0, 1994a.

Pankow, J. F.: An absorption model of the gas/aerosol partitioning involved in the formation of secondary organic aerosol, Atmos. Environ., 28(2), 189–193, doi:10.1016/1352-2310(94)90094-9, 1994b.

Pankow, J. F., Seinfeld, J. H., Asher, W. E. and Erdakos, G. B.: Modeling the formation of secondary organic aerosol. 1. Application of theoretical principles to measurements obtained in the α-pinene/, β-pinene/, sabinene/, Δ3-carene/, and cyclohexene/ozone systems, Environ. Sci. Technol., 35(6), 1164–1172, doi:10.1021/es001321d, 2001.

Renbaum-Wolff, L., Grayson, J. W., Bateman, A. P., Kuwata, M., Sellier, M., Murray, B. J., Shilling, J. E., Martin, S. T. and Bertram, A. K.: Viscosity of α-pinene secondary organic material and implications for particle growth and reactivity., Proc. Natl. Acad. Sci. U. S. A., 110(20), 8014–8019, doi:10.1073/pnas.1219548110, 2013.

Schobesberger, S., D'Ambro, E. L., Lopez-Hilfiker, F. D., Mohr, C. and Thornton, J. A.: A model framework to retrieve thermodynamic and kinetic properties of organic aerosol from composition-resolved thermal desorption measurements, Atmos. Chem. Phys., 18(20), 14757–14785, doi:10.5194/acp-18-14757-2018, 2018.

Stark, H., Yatavelli, R. L. N., Thompson, S. L., Kang, H., Krechmer, J. E., Kimmel, J. R., Palm, B. B., Hu, W., Hayes, P. L., Day, D. A., Campuzano-Jost, P., Canagaratna, M. R., Jayne, J. T., Worsnop, D. R. and Jimenez, J. L.: Impact of Thermal Decomposition on Thermal Desorption Instruments: Advantage of Thermogram Analysis for Quantifying Volatility Distributions of Organic Species, Environ. Sci. Technol., 51(15), 8491–8500, doi:10.1021/acs.est.7b00160, 2017.

Surratt, J. D., Lewandowski, M., Offenberg, J. H., Jaoui, M., Kleindienst, T. E., Edney, E. O. and Seinfeld, J. H.: Effect of acidity on secondary organic aerosol formation from isoprene, Environ. Sci. Technol., 41(15), 5363–5369,

doi:10.1021/es0704176, 2007.

Tikkanen, O., Buchholz, A., Ylisirniö, A., Schobesberger, S. and Virtanen, A.: Comparing SOA volatility distributions derived from isothermal SOA particle evaporation data and FIGAERO-CIMS measurements, Atmos. Chem. Phys. Discuss., (November), 1–34, doi:10.5194/acp-2019-927, 2019.

5   Tolocka, M. P., Jang, M., Ginter, J. M., Cox, F. J., Kamens, R. M. and Johnston, M. V.: Formation of Oligomers in Secondary Organic Aerosol, Environ. Sci. Technol., 38(5), 1428–1434, doi:10.1021/es035030r, 2004.

Ulbrich, I. M., Canagaratna, M. R., Zhang, Q., Worsnop, D. R. and Jimenez, J. L.: Interpretation of organic components from Positive Matrix Factorization of aerosol mass spectrometric data, Atmos. Chem. Phys., 9(9), 2891–2918, doi:10.5194/acp-9-2891-2009, 2009.

10 Virtanen, A., Joutsensaari, J., Koop, T., Kannosto, J., Yli-Pirilä, P., Leskinen, J., Mäkelä, J. M., Holopainen, J. K., Pöschl, U., Kulmala, M., Worsnop, D. R. and Laaksonen, A.: An amorphous solid state of biogenic secondary organic aerosol particles, Nature, 467(7317), 824–827, doi:10.1038/nature09455, 2010.

Wang, D. S. and Hildebrandt Ruiz, L.: Chlorine-initiated oxidation of alkanes under high-NO conditions: Insights into secondary organic aerosol composition and volatility using a FIGAERO-CIMS, Atmos. Chem. Phys., 18(21), 15535–
15 15553, doi:10.5194/acp-18-15535-2018, 2018.

Wilson, J., Imre, D., Beránek, J., Shrivastava, M. and Zelenyuk, A.: Evaporation kinetics of laboratory-generated secondary organic aerosols at elevated relative humidity, Environ. Sci. Technol., 49(1), 243–249, doi:10.1021/es505331d, 2015.

Yan, C., Nie, W., Äijälä, M., Rissanen, M. P., Canagaratna, M. R., Massoli, P., Junninen, H., Jokinen, T., Sarnela, N.,
20 Häme, S. A. K., Schobesberger, S., Canonaco, F., Yao, L., Prévôt, A. S. H., Petäjä, T., Kulmala, M., Sipilä, M., Worsnop, D. R. and Ehn, M.: Source characterization of highly oxidized multifunctional compounds in a boreal forest environment using positive matrix factorization, Atmos. Chem. Phys., 16(19), 12715–12731, doi:10.5194/acp-16-12715-2016, 2016.

Yli-Juuti, T., Pajunoja, A., Tikkanen, O. P., Buchholz, A., Faiola, C., Väisänen, O., Hao, L., Kari, E., Peräkylä, O., Garmash, O., Shiraiwa, M., Ehn, M., Lehtinen, K. and Virtanen, A.: Factors controlling the evaporation of secondary
25 organic aerosol from a-pinene ozonolysis, Geophys. Res. Lett., 44(5), 2562–2570, doi:10.1002/2016GL072364, 2017.

6   Tables

Table 1: Signal weighted average values of elemental composition, O:C, OSc, and contribution of C>10 compounds for all factors.

ID	composition	M_w / g mol^{-1}	O:C	OSc	C>10 / %
LV1	$C_{8.6}H_{13.3}O_{5.2}$	213.4	0.66	-0.27	9.3
LV2	$C_{9.0}H_{14.2}O_{5.6}$	200.3	0.64	-0.30	12.7
LV3	$C_{10.3}H_{16.7}O_{6.8}$	249.7	0.70	-0.21	36.5
LV4	$C_{12.6}H_{21.8}O_{7.9}$	300.5	0.66	-0.39	65.2
LV5	$C_{12.5}H_{21.3}O_{8.5}$	308.2	0.72	-0.24	65.1
LD1	$C_{9.8}H_{15.4}O_{6.3}$	235.7	0.74	-0.05	33.8
LB1	$C_{9.7}H_{15.5}O_{6.2}$	234.8	0.78	0.00	38.3
LC1	$C_{8.6}H_{14.3}O_{5.2}$	201.9	0.81	-0.05	28.2
LC2	$C_{6.2}H_{9.5}O_{3.9}$	148.0	0.93	0.21	7.6
MV1	$C_{7.8}H_{11.6}O_{5.0}$	185.8	0.70	-0.12	7.6
MV2	$C_{8.1}H_{11.6}O_{5.8}$	202.3	0.76	0.07	4.1
MV3	$C_{9.0}H_{13.4}O_{6.5}$	226.6	0.76	0.01	15.4
MV4	$C_{10.1}H_{16.0}O_{7.4}$	257.1	0.80	0.02	38.3
MV5	$C_{11.3}H_{18.7}O_{7.6}$	276.5	0.73	-0.17	51.4
MD1	$C_{8.8}H_{13.5}O_{5.9}$	214.8	0.75	-0.01	7.6
MB1	$C_{9.8}H_{15.6}O_{6.1}$	235.5	0.79	0.02	38.9
HV1	$C_{7.0}H_{9.5}O_{5.6}$	184.7	0.90	0.43	6.2
HV2	$C_{7.9}H_{11.1}O_{6.3}$	208.6	0.86	0.29	8.5
HV3	$C_{7.7}H_{10.6}O_{6.3}$	204.3	0.92	0.44	12.9
HV4	$C_{8.4}H_{12.4}O_{6.6}$	219.4	0.87	0.23	18.6
HV5	$C_{10.0}H_{16.2}O_{6.8}$	247.4	0.76	-0.09	39.8
HD1	$C_{8.3}H_{12.3}O_{5.9}$	207.1	0.82	0.18	19.7
HB1	$C_{9.7}H_{15.5}O_{6.1}$	232.8	0.77	-0.02	38.4

Table 2: T_{max} values for all V-type factors. "-" indicates that there was not enough signal to determine T_{max} values.

ID	dry, t_{evap}=0.25h	dry, t_{evap}=4h	80%, t_{evap}=0.25h	80%, t_{evap}=4h
LV1	37.4	42.5	44.7	-
LV2	51.7	56.5	56.0	56.8
LV3	66.5	70.3	71.2	69.2
LV4	82.0	83.6	86.5	86.6
LV5	95.8	97.6	99.3	102.7
MV1	42.9	44.1	48.1	-
MV2	59.7	58.2	63.7	63.2
MV3	74.9	73.5	78.7	79.6
MV4	93.6	91.6	97.3	101.1
MV5	118.8	116.5	122.5	129.9
HV1	60.7	61.0	75.3	-
HV2	77.2	76.7	93.7	136.5
HV3	58.1	60.0	87.8	104.3
HV4	95.8	94.7	109.0	128.5
HV5	121.6	120.3	136.5	148.0

7   Figures
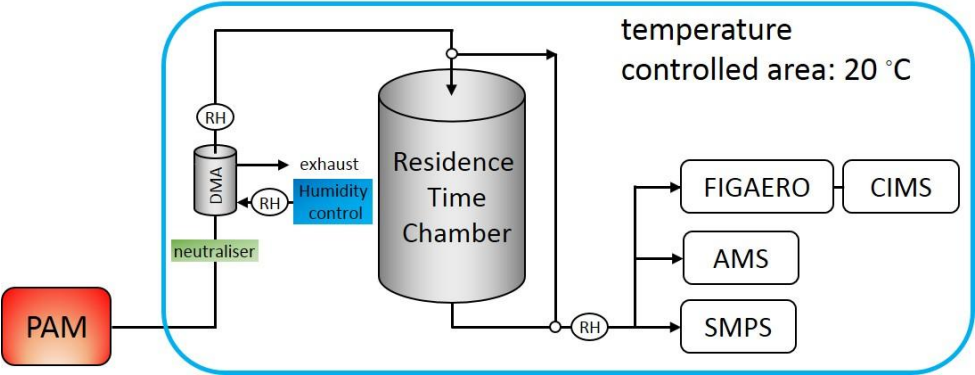
Figure 1: Schematic of experimental setup.
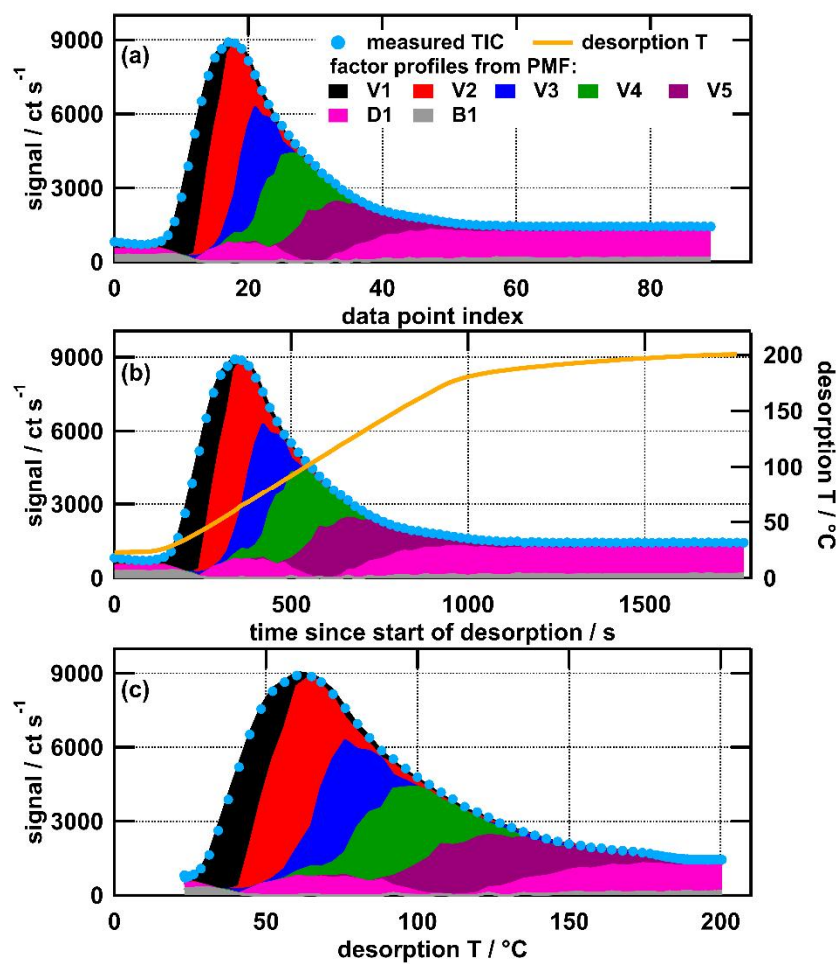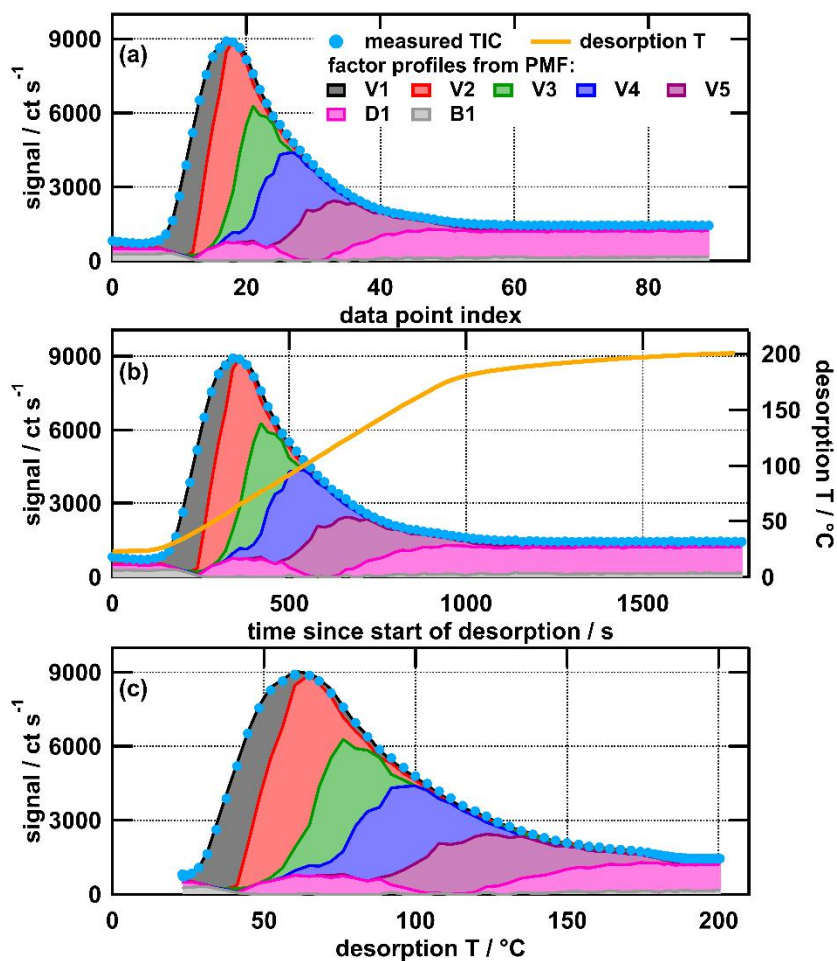
Figure 2: Measured total ion thermogram colour coded with the contribution of PMF model output factors for the mediumOC, $t_{evap} = 4$ h, wet case plotted vs data point index (a), time since start of desorption (b), and desorption temperature (c). Note that the desorption temperature ramp (b) is not increasing linearly after ~1000 s. This "soak" period ensures that all organic material is removed from the filter before the next collection.
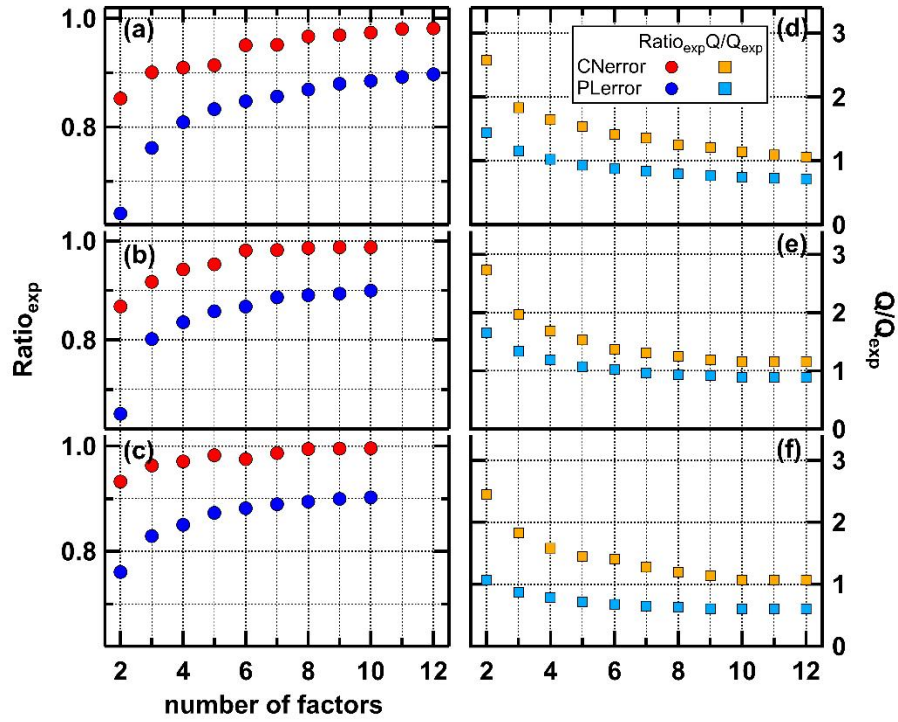
Figure 3: Fraction of explained variance (*Ratio_exp*, left) and *Q/Q_exp* values (right) for the low- (a), medium- (b) and highOC- dataset for PLerror (blue) and CNerror(red).
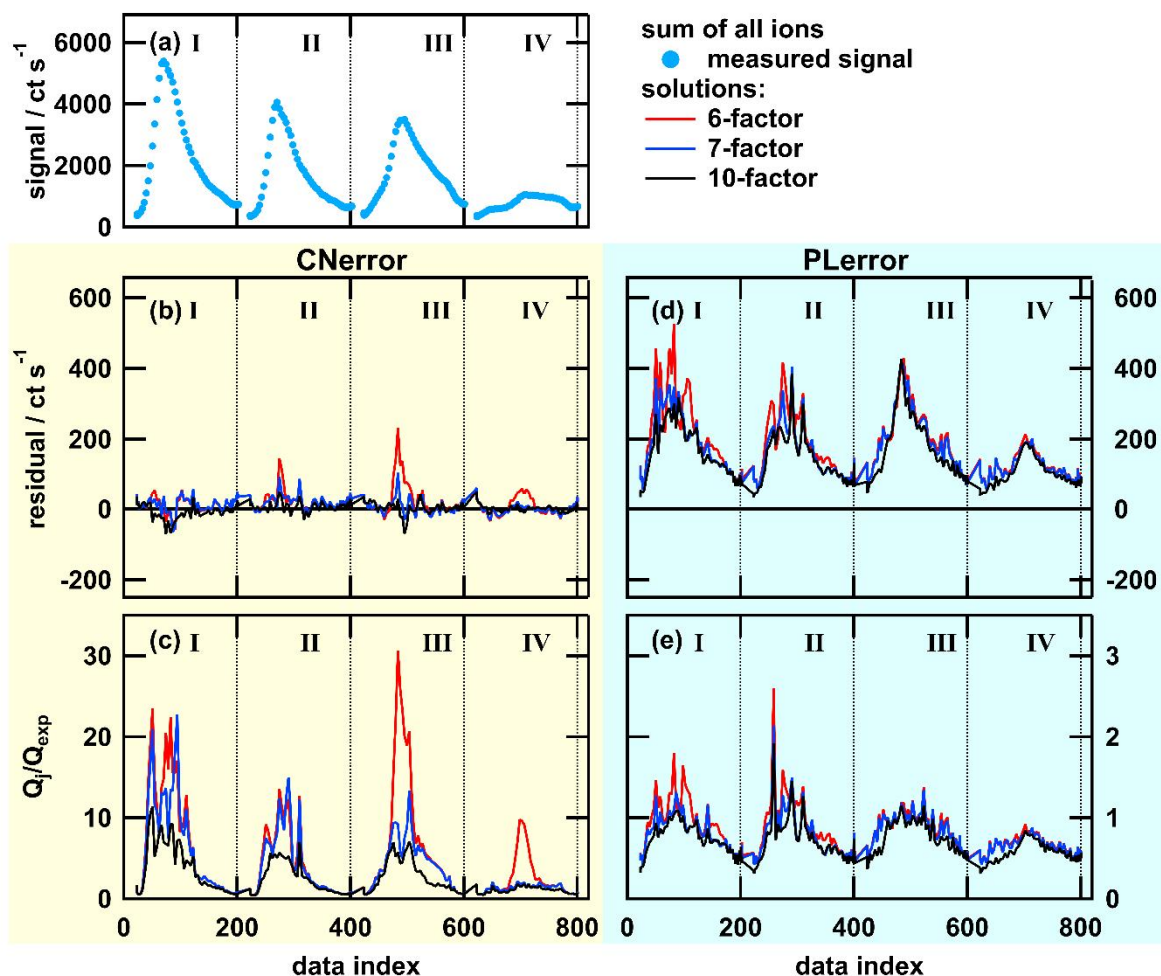
Figure 4: Total ion thermogram (a), residuals (b and d) and Q_j/Q_{exp} values (c and e) as time series for solutions with 6, 7, or 10 factors for PMF run with CNerror (b and c, yellow background) and PLerror (d and e, blue background). The dataset contains thermogram scans for highOC SOA particles of these sampling conditions: dry, t_{evap} = 0.25 h (I), dry, t_{evap} = 4 h(II), wet, t_{evap} = 0.25 h (III), and wet, t_{evap} = 4 h (IV). Note that the y scaling is the same in panels (b) and (d), but in (e) it is 10 times smaller than in (c).
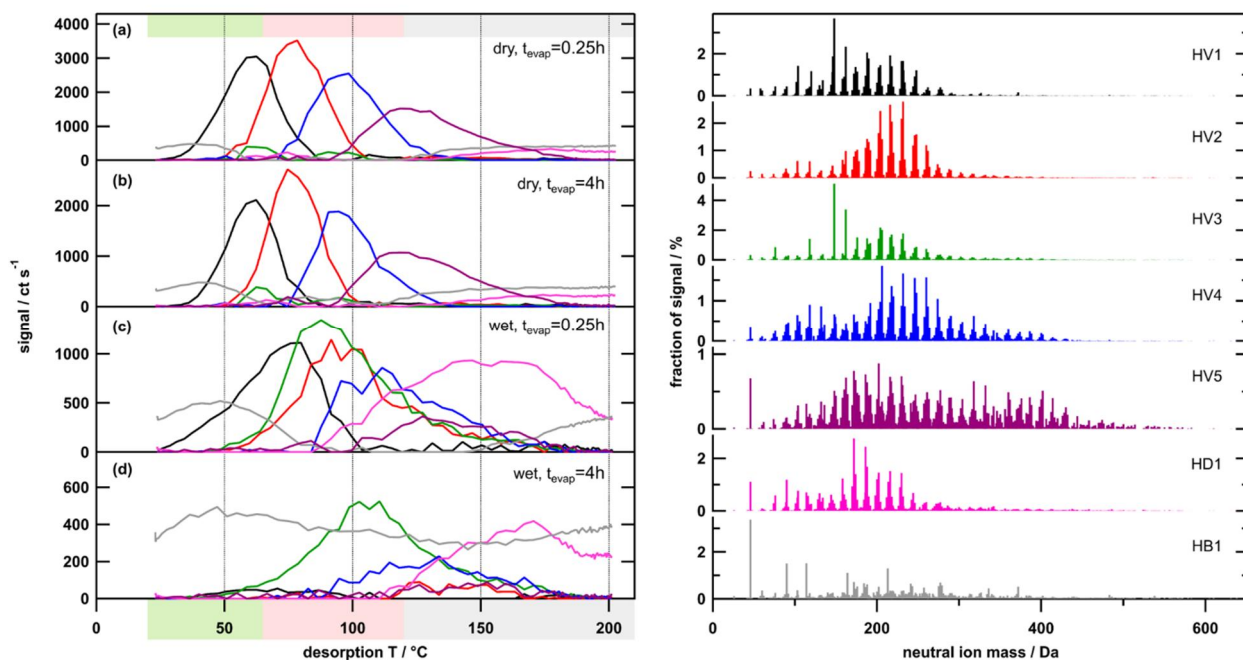
5

31
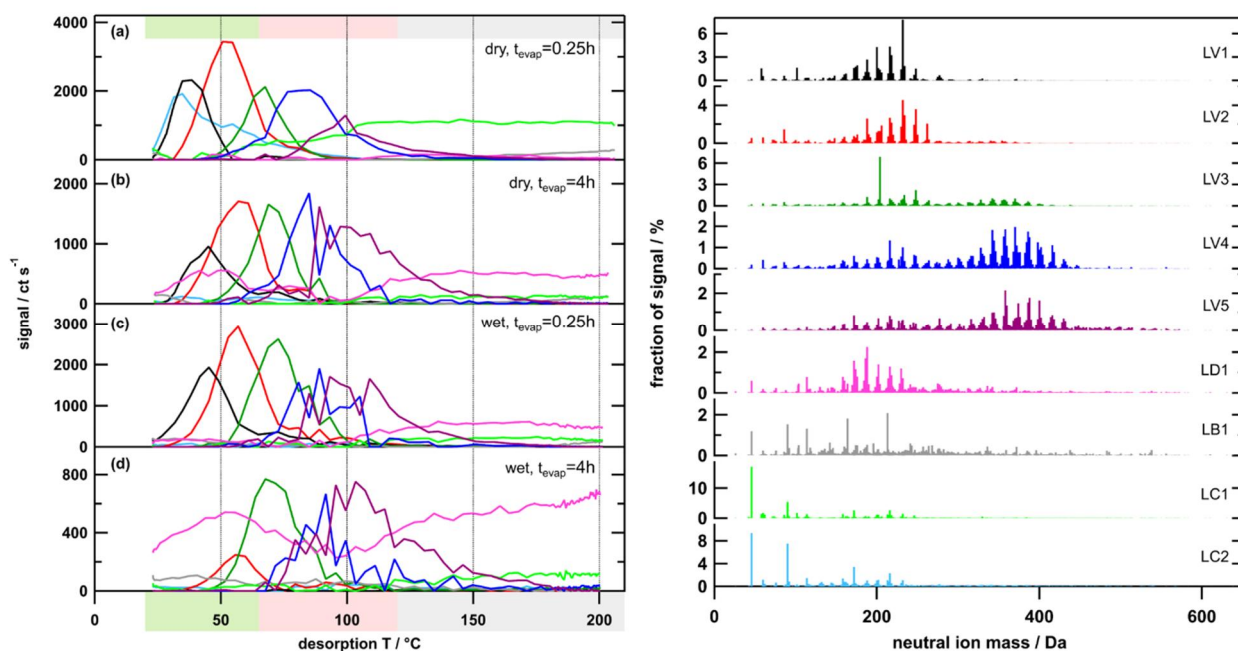
Figure 5: Temperature profiles (left) and factor mass spectra (right) for the 9-factor solution for the lowOC case. Each factor mass spectrum is normalised. The colour code is the same for both panels. Background colours in the left panel indicate volatility classifications according to Donahue et al. (2006) derived from T_{max}-C^* calibrations (green: SVOC, red: LVOC, grey: ELVOC). Note the different scaling for y-axes in panels a-d.
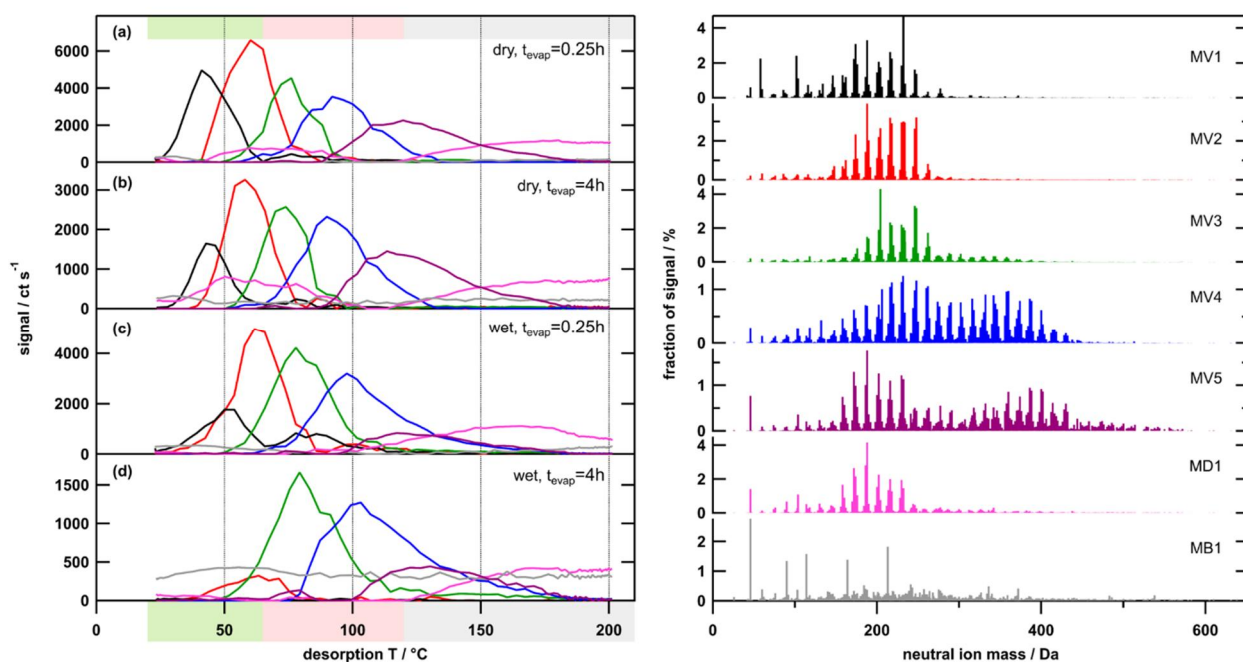
Figure 6: Temperature profiles (left) and factor mass spectra (right) for the 7-factor solution for the mediumOC case. Each factor mass spectrum is normalised. The colour code is the same for both panels. Background colour in the left panel indicates volatility classification derived from T_{max}-C* calibrations (green: SVOC, red: LVOC, grey: ELVOC). Note the different scaling for y-axes in panels a-d.

Figure 7: Temperature profiles (left) and factor mass spectra (right) for the 7-factor solution for highOC case. Each factor mass spectrum is normalised. The colour code is the same for both panels Background colour in the left panel indicates volatility classification derived from T_{max} - C^* calibrations (green: SVOC, red: LVOC, grey: ELVOC). Note the different scaling for y-axes in panels a-d.
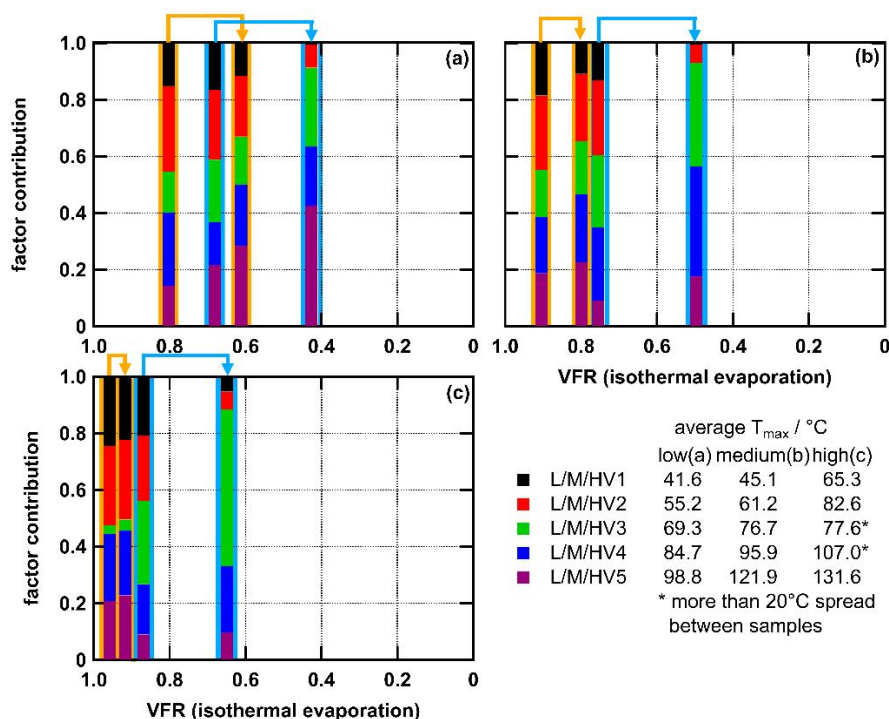
Figure 8: Contribution of type V factors to total signal for low- (a), medium- (b), and highOC cases (c). The x-axis is the average volume fraction remaining (VFR) after comparable time intervals of isothermal evaporation observed measured in separate RTC experiments. Orange and blue arrows indicate the change from $t_{evap} = 0.25$ h to $t_{evap} = 4$ h particles for dry and wet conditions, respectively. Note that the colour code is the same in all panels, but LV1 is not equal to MV1 etc. VFR values are from isothermal evaporation measurements described in Buchholz et al. (2019). Average T_{max} values are for comparison of the volatility of the factors. Detailed values are given in Table 2.
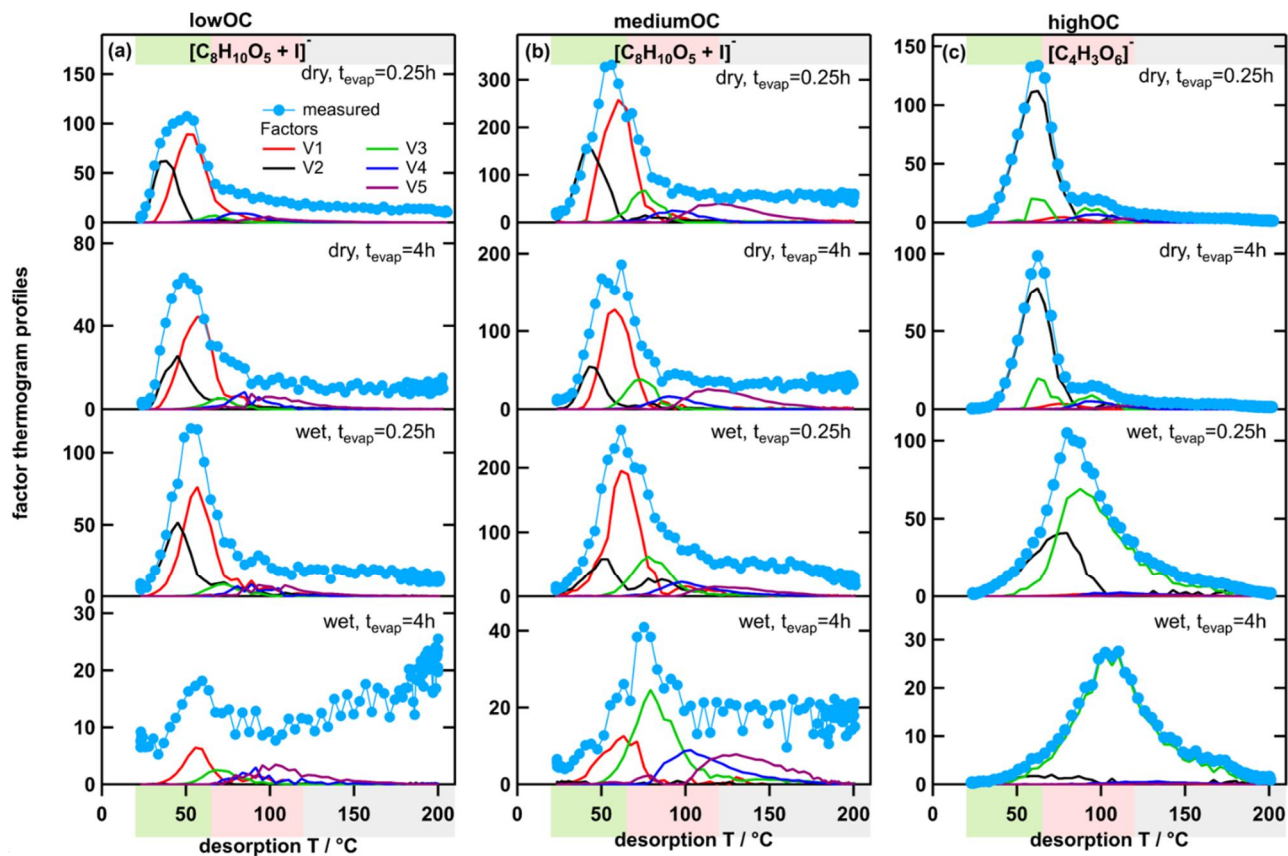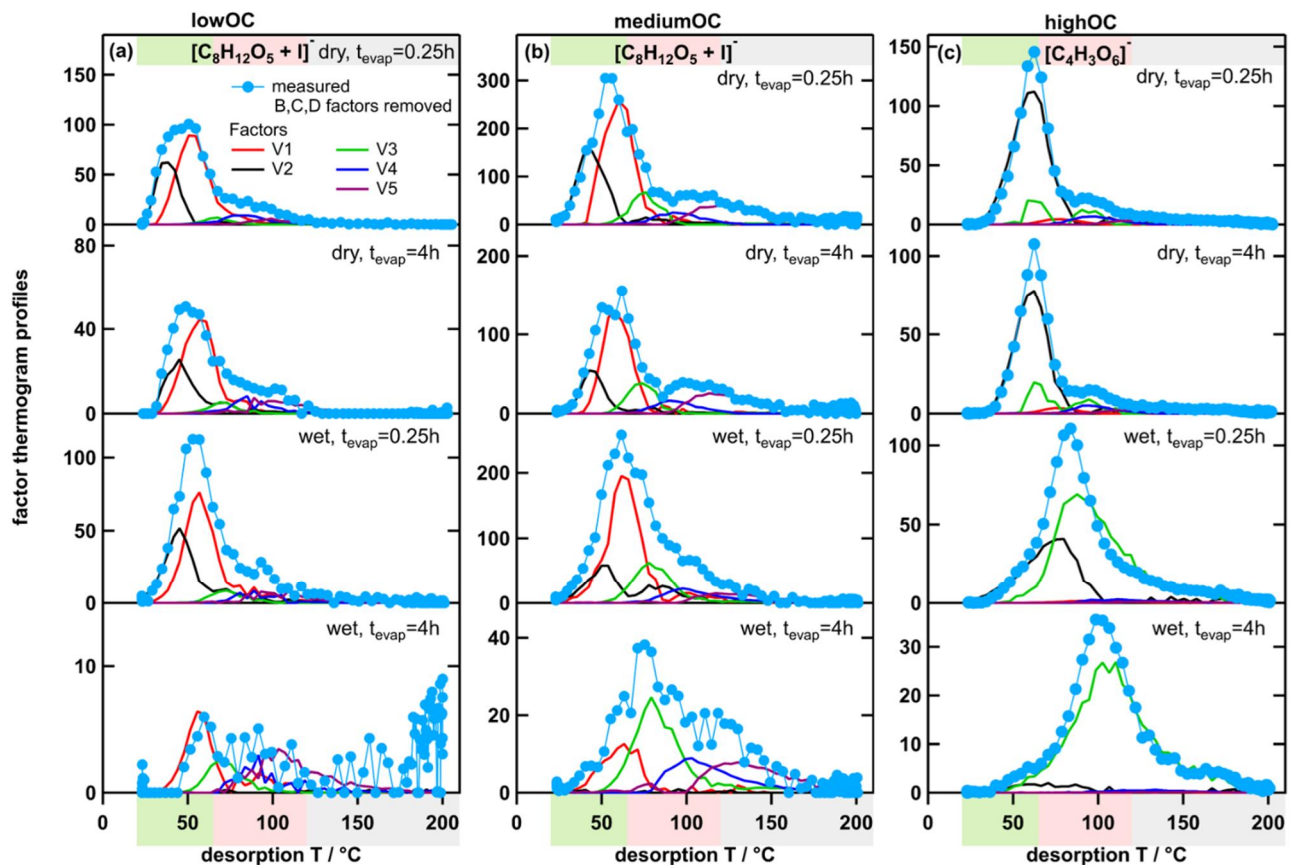
Figure 9: Measured ion thermograms and factor thermogram profiles for ion $[C_8H_{12}O_5+I]^-$ in the low- (a) and mediumOC cases (b) and $C_4H_3O_6^-$ in the highOC case (c). Note that to reduce clutter in the graph only V-type factors are displayed. Thus, coloured lines will not add up to the measured values (light blue) if the sample to background ratio was low (e.g. bottom panel in a).
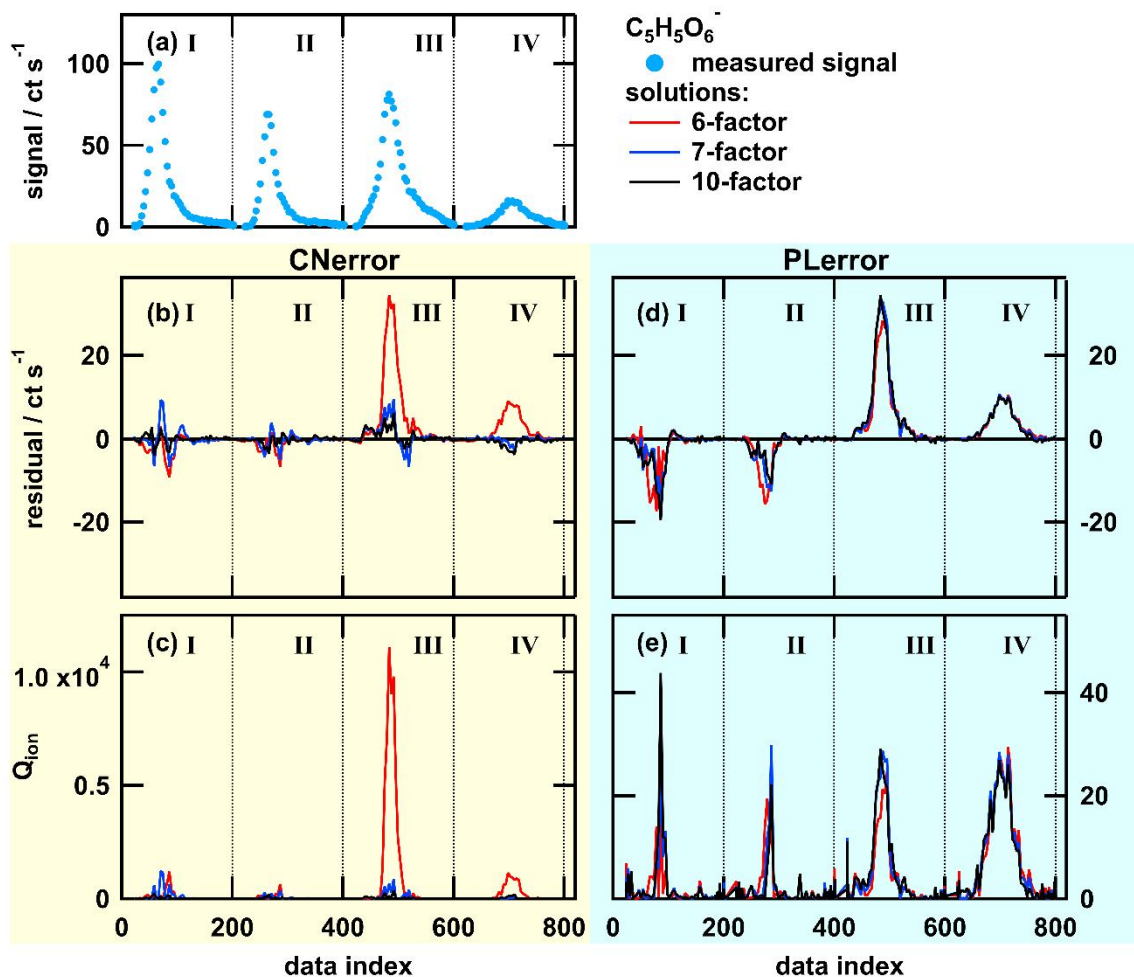
Figure A 1: Single ion thermogram (a), residual (b and d), and Q_{ion} values (c and e) as time series for solutions with 6, 7, or 10 factors for PMF run with CNerror (b and c) and PLerror (d and e) for the ion $C_5H_5O_6^-$. The dataset contains thermogram scans for highOC SOA particles of these sampling conditions: dry, $t_{evap} = 0.25$ h (I), dry, $t_{evap} = 4$ (II), wet, $t_{evap} = 0.25$ h (III), and wet, $t_{evap} = 4$ h (IV). Note that the y scaling is the same in panels (b) and (d) but in (e) it is much smaller than in (c).
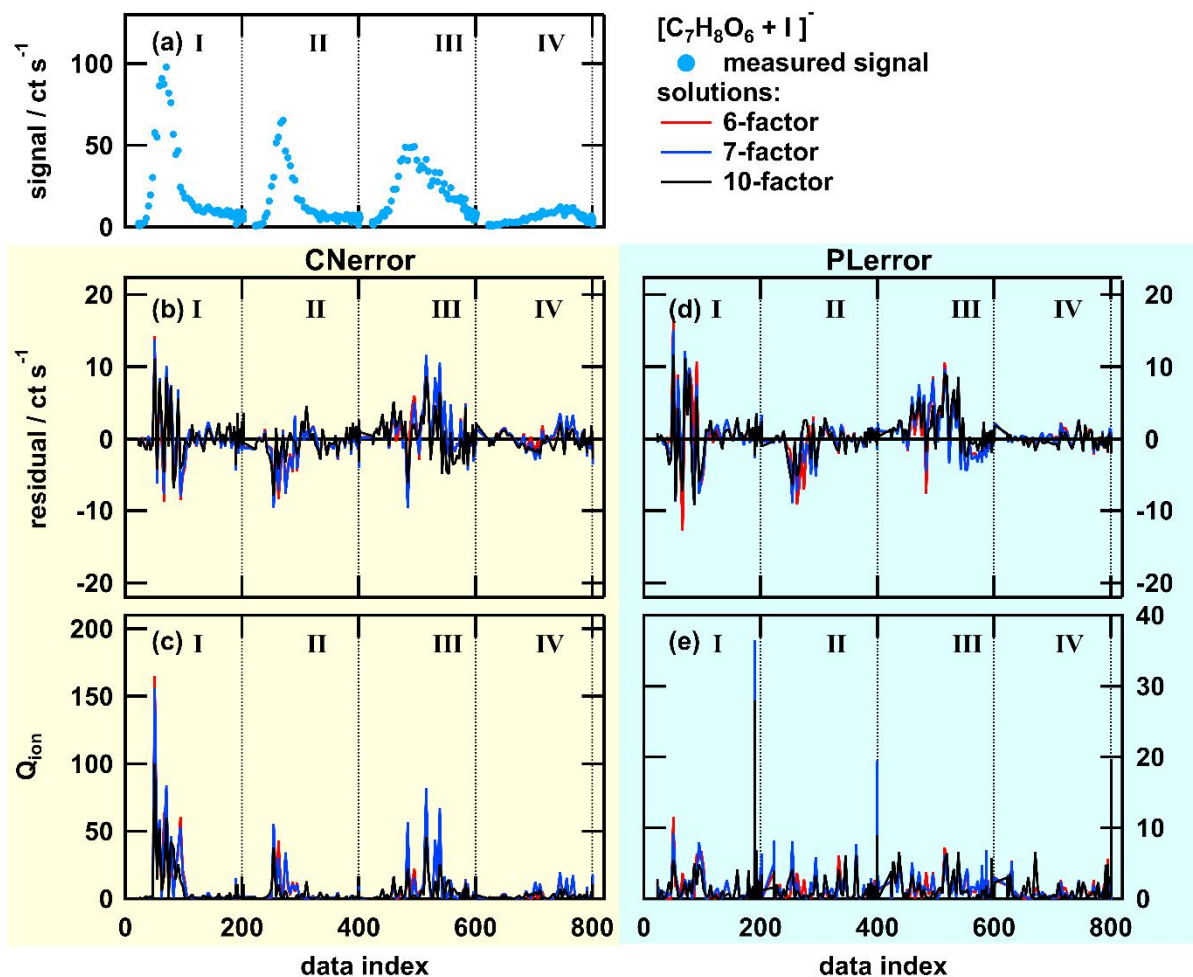
Figure A 2: Single ion thermogram (a), residuals (b and d), and Q_{ion} values (c and e) as time series for solutions with 6, 7, or 10 factors for PMF run with CNerror (b and c) and PLerror (d and e) for the ion $[C_7H_8O_6 + I]^-$. The dataset contains thermogram scans for highOC SOA particles of these sampling conditions: dry, $t_{evap} = 0.25$ h (I), dry, $t_{evap} = 4$ h (II), wet, $t_{evap} = 0.25$ h (III), and wet, $t_{evap} = 4$ h (IV). Note that the y scaling in (e) is much smaller than in (c).
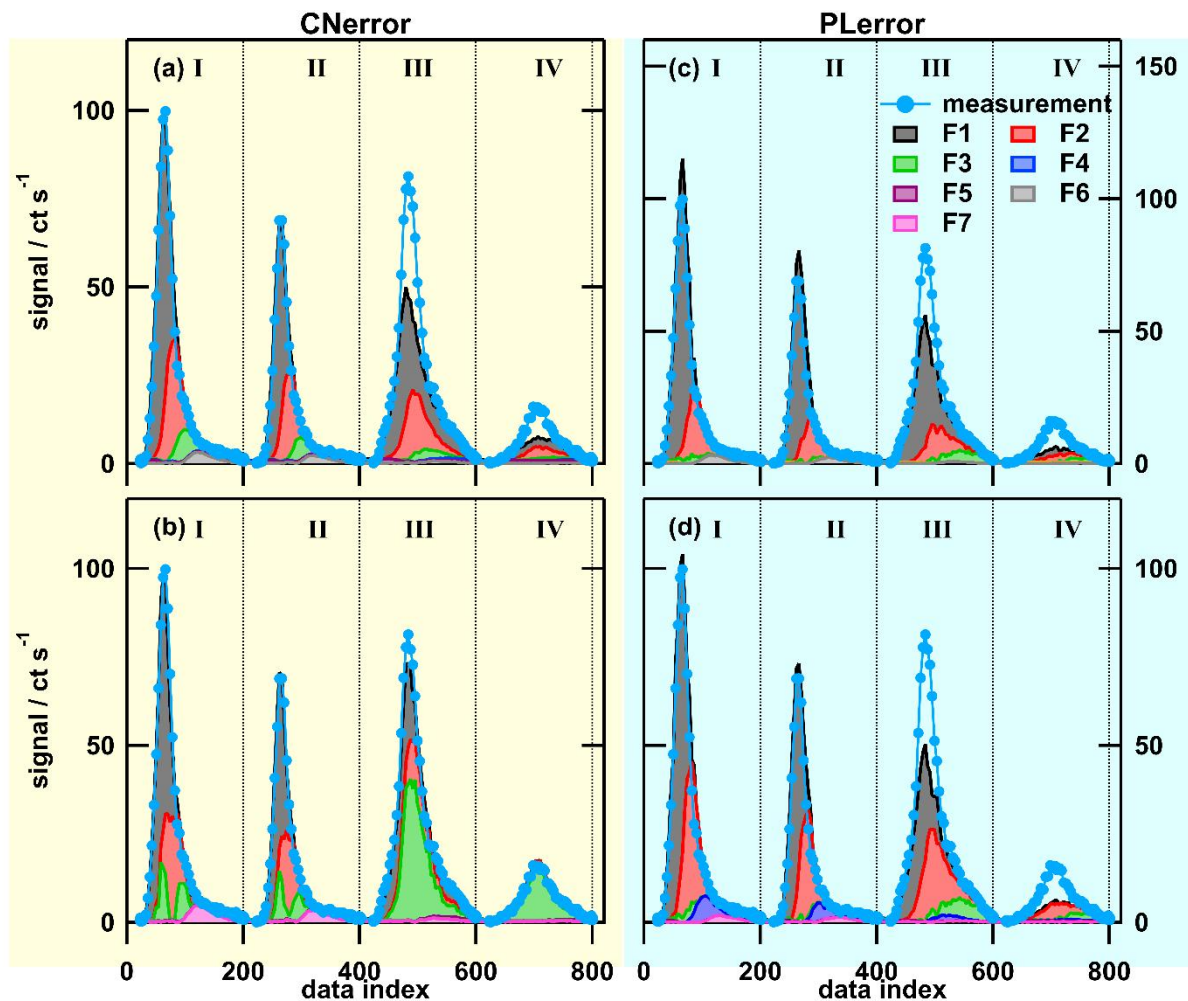
Figure A 3: Combined single ion thermograms of the ion $C_5H_5O_6^-$ for PMF factor profiles for 6 (a and c) and 7 (b and d) factor solution. Left column (a and b) are calculated with CNerror, right column (c and d) with PLerror. The dataset contains thermogram scans for highOC SOA particles of these sampling conditions: dry, $t_{evap} = 0.25$ h (I), dry, $t_{evap} = 4$ h (II), wet, $t_{evap} = 0.25$ h (III), and wet, $t_{evap} = 4$ h (IV). Note that generally the factors are not the same between the two error schemes or the two solutions (i.e., F1 in the 6-factor solution with CNerror is different from F1 in the 7-factor solution with CNerror etc.)